G6P-capturing molecules in the periplasm of Escherichia coli accelerate the shikimate pathway

Fujiwara, Ryosuke ; Nakano, Mariko ; Hirata, Yuuki ; Otomo, Chisako ; Nonaka, Daisuke ; Kawada, Sakiya ; Nakazawa, Hikaru ; Umetsu, Mitsuo ;…

(Citation)
Metabolic Engineering,72:68-81

(Issue Date)
2022-07

(Resource Type)
journal article

(Version)
Accepted Manuscript

Highlights

- Periplasmic expression of β-glucosidase (BGL) increases L-Phe production in *E. coli*
- Two key factors involved in this phenomenon, G6P and $EIIC^{Glc}$ domain, were defined
- Cytoplasmic G6P is secreted into the periplasm via $EIIC^{Glc}$ domain and captured by BGL
- Periplasmic expression of other G6P-capturing proteins also increase L-Phe production
- This technique can be applied to produce other shikimate pathway derivatives

Author Contributions

Ryosuke Fujiwara: Conceptualization, Methodology, Formal Analysis, Investigation, Writing–Original Draft.

Mariko Nakano: Investigation.

Yuuki Hirata: Investigation.

Chisako Otomo: Investigation.

Daisuke Nonaka: Investigation.

Sakiya Kawada: Investigation.

Hikaru Nakazawa: Investigation.

Mitsuo Umetsu: Investigation.

Tomokazu Shirai: Methodology.

Shuhei Noda: Conceptualization, Methodology, Formal Analysis, Investigation, Writing–Review & Editing.

Tsutomu Tanaka: Conceptualization, Methodology, Formal Analysis, Investigation, Writing–Review & Editing.

Akihiko Kondo: Supervision

G6P-capturing molecules in the periplasm of *Escherichia coli* accelerate the shikimate pathway

Ryosuke Fujiwara[a,†], Mariko Nakano[a], Yuuki Hirata[a], Chisako Otomo[a], Daisuke Nonaka[a], Sakiya Kawada[b], Hikaru Nakazawa[b], Mitsuo Umetsu[b], Tomokazu Shirai[c], Shuhei Noda[c,*] Tsutomu Tanaka[a,*], Akihiko Kondo[c,d]

[a]Department of Chemical Science and Engineering, Graduate School of Engineering, Kobe University, 1-1 Rokkodai, Nada, Kobe 657-8501, Japan

[b]Department of Biomolecular Engineering Graduate School of Engineering, Tohoku University, 6-6-11 Aoba, Aramaki, Aoba-ku, Sendai 980-8579, Japan

[c]Center for Sustainable Resource Science, RIKEN, 1-7-22 Suehiro-cho, Tsurumi-ku, Yokohama, Kanagawa 230-0045, Japan

[d]Graduate School of Science, Technology and Innovation, Kobe University, 1-1 Rokkodai, Nada, Kobe 657-8501, Japan

†Current address: R. Fujiwara Center for Sustainable Resource Science, RIKEN, 1-7-22 Suehiro-cho, Tsurumi-ku, Yokohama, Kanagawa 230-0045, Japan

Corresponding authors:

* Shuhei Noda, **Email:** shuhei.noda@riken.jp

* Tsutomu Tanaka, **Email:** tanaka@kitty.kobe-u.ac.jp

Abstract

Escherichia coli, the most studied prokaryote, is an excellent host for producing valuable chemicals from renewable resources as it is easy to manipulate genetically. Since the periplasmic environment can be easily controlled externally, elucidating how the localization of specific proteins or small molecules in the periplasm affects metabolism may lead to bioproduction development using *E. coli*. We investigated metabolic changes and its mechanisms occurring when specific proteins are localized to the *E. coli* periplasm. We found that the periplasmic localization of β-glucosidase promoted the shikimate pathway involved in the synthesis of aromatic chemicals. The periplasmic localization of other proteins with an affinity for glucose-6-phosphate (G6P), such as inactivated mutants of Pgi, Zwf, and PhoA, similarly accelerated the shikimate pathway. Our results indicate that G6P is transported from the cytoplasm to the periplasm by the glucose transporter protein $EIICB^{Glc}$, and then captured by β-glucosidase.

Keywords

Periplasm, shikimate pathway, *Escherichia coli*, glucose-6-phosphate, phosphotransferase system

Introduction

Technologies allowing for the bioproduction of fuels and chemicals from renewable resources are in great demand. Extensive research efforts aim to develop technologies to produce aromatic compounds for chemical, pharmaceutical, food, feed, and other industries (Fujiwara et al., 2018; Shen et al., 2017; Sun et al., 2016). In *Escherichia coli*, most aromatic chemicals are synthesized endogenously through the shikimate pathway (Noda and Kondo, 2017). Production of shikimate derivatives could be increased by promoting the shikimate pathway (Nakagawa et al., 2011) and/or disrupting the competing pathways (Niu et al., 2019; Noda et al., 2016; Rodriguez et al., 2013). For example, salicylate, an important chemical in the pharmaceutical industry, is a main shikimate pathway derivative (Noda et al., 2016). Phenol and styrene, which have major industrial applications worldwide, can also be produced using microbial catalysis under moderate reaction conditions (Chung et al., 2015; Lian et al., 2016). The aromatic amino acids L-phenylalanine (Phe), L-tyrosine (Tyr), and L-tryptophan (Trp) are produced via enzymatic reactions from chorismate, the end product of the shikimate pathway (Lütke-Eversloh and Stephanopoulos, 2007; Olson et al., 2007; Wu et al., 2018). Important dicarboxylic acids as raw materials for polymers with high industrial demand, such as *cis*,*cis*-muconic acid (MA) and maleate, could also be obtained from chorismate (Fujiwara et al., 2018; Noda et al., 2016; Thompson et al., 2018; Zhang et al., 2015). Therefore, the microbial production of shikimate pathway derivatives represents a potentially game-changing technology for both the environment and economy.

The periplasm is a space between the inner and outer membranes of gram-negative bacteria, which generally contains a peptidoglycan layer. Estimates of periplasmic thickness in *E. coli* vary from 10 to 50 nm (Sochacki et al., 2011), accounting for approximately 20%–40% of their cellular volume (Stock et al., 1977). The periplasm of *E. coli* contains > 60 known proteins, including amino acid-, sugar-, vitamin-, and ion-binding proteins; degradative enzymes (phosphatases, proteases, and endonucleases); and antibiotic detoxifying enzymes. (Schmidt T., 2019). In bioproduction using bacteria, the periplasm is used as a localization site for proteins during heterologous protein production (Bodelón et al., 2013; Fernández, 2004; Malherbe et al., 2019) or as a localization site for hydrolases to provide bacteria the ability to use carbon sources that are originally unavailable (Georgiou and Segatori, 2005; Kurumbang et al., 2020). In *E. coli*, periplasmic expression of Tfu0937, a β-glucosidase (BGL) from *Thermobifida fusca* YX that hydrolyzes β-glycosidic bonds in cellobiose and cello-oligosaccharides, has been used for the production of valuable chemicals from cello-oligosaccharides (Tanaka et al., 2011). For instance, periplasmic BGL expression has been used to produce mevalonate and 1,2-propanediol from cellobiose (Nonaka et al., 2021; Satowa et al., 2020). Although periplasmic protein expression methods are now well-established (Gonzalez-Perez et al., 2021; Mirzadeh et al., 2020), the mechanisms by which periplasmic expression of proteins such as BGL affect metabolism remain largely undetermined.

Here, we demonstrate that the periplasmic expression of BGL or inactivated BGL increased L-phenylalanine (Phe) production from glucose. We investigated factors related to this phenomenon and found that $EIICB^{Glc}$ and glucose-6-phosphate (G6P) were

involved. *E. coli* with heterologous BGL expression exhibited accumulation of intracellular phosphoenolpyruvate (PEP), which accelerates the shikimate pathway. We hypothesized that G6P is transported from the cytoplasm to the periplasm by $EIICB^{Glc}$ and then captured by BGL in the periplasm. We confirmed that periplasmic expression of other proteins that capture G6P also increases Phe production, thus supporting our hypothesis. Furthermore, the production of other shikimate pathway derivatives, Tyr and MA, was also increased by the method expressing BGL in the periplasm.

Material and methods

Media

Lysogeny broth (LB) medium comprising 10 g L^{-1} tryptone, 5 g L^{-1}yeast extract, and 5 g L^{-1} NaCl was used for preculture. For L-phenylalanine and MA production, a modified M9 medium was used. The M9 minimal medium (0.5 g L^{-1}NaCl, 17.1 g L^{-1} Na_2HPO_4•$12H_2O$, 3 g L^{-1} KH_2PO_4, 1 g L^{-1} NH_4Cl, 246 mg L^{-1} $MgSO_4$•$7H_2O$, 14.7 mg L^{-1} $CaCl_2$•$2H_2O$, 2.78 mg L^{-1} $FeSO_4$•$7H_2O$, 10 mg L^{-1} thiamine hydrochloride) was supplemented with 5 g L^{-1} yeast extract, 10 mM sodium pyruvate, a carbon source (20 g L^{-1} glucose, xylose or fructose), 40 mg L^{-1} L-tyrosine and 40 mg L^{-1} of L-tryptophan. The inclusion of L-tyrosine and L-tryptophan aimed to prevent auxotrophic effects of the ATCC31882 strain on these amino acids. For L-tyrosine production, a modified M9 medium supplemented with 100 mg L^{-1} L-phenylalanine without adding L-tyrosine was used. When comparing the capability of glucose and G6P as carbon sources, 55.5 mM of these components were added to this modified M9 medium. For L-tyrosine production, a modified M9 medium supplemented with 10 g L^{-1} glucose was instead used. Ampicillin,

kanamycin or chloramphenicol were added to the media with a final concentration of 100, 20 or 30 mg L^{-1}, respectively.

Culture conditions

Engineered strains were precultured in test tubes containing LB medium for one day at 37°C with shaking at 220 rpm. Each preculture medium was centrifuged at 12,000 × g for 3 min and the pellet washed with M9 minimal medium without sugars. The preculture was then used to inoculate the appropriate media at an initial optical density of 0.1, measured at a wavelength of 600 nm (OD_{600}). As needed, 0.1 mM isopropyl β-D-1-thiogalactopyranoside (IPTG) was also added to the media. Test tube-scale cultures were incubated at 37°C with shaking at 220 rpm.

Strains and plasmid construction

Supplementary Table 1 lists the strains and plasmids used in this study. *Escherichia coli* NovaBlue competent cells (Novagen, Cambridge, MA, USA) were employed for gene cloning. We conducted polymerase chain reaction (PCR) using KOD FX Neo (Toyobo, Osaka, Japan) and synthesis of custom DNA oligonucleotide primers using Invitrogen custom DNA oligos (Thermo Fisher Scientific, Tokyo, Japan) (Supplementary Table 2). The In-Fusion HD Cloning Kit (Takara Bio, Shiga, Japan) was used to assemble multiple DNA fragments and circularize linearized DNA fragments. Supplementary Table 3 summarizes the detailed construction methods for all plasmids.

Deletion of chromosomal genes

Supplementary Table 1 lists the plasmids used to delete chromosomal genes. The deletion strains were constructed in this study using the CRISPR-Cas two-plasmid system (Jiang *et al.*, 2015). A pCas plasmid was first introduced in the parental strain. Subsequently, an appropriate pTΔ plasmid was introduced in the pCas-harboring strain, followed by overnight incubation in LB medium with 10 g L^{-1} arabinose as an inducer for λ-Red, without kanamycin or spectinomycin. The culture was plated on LB agar containing 50 mg L^{-1} kanamycin and 100 mg L^{-1} spectinomycin after culture recovery. Targeted gene deletion was confirmed using colony PCR and the plasmids pCas and pTΔ were eliminated from the bacterial target-gene-deficient strain. All fragments inserted in the plasmids to inactivate respective genes were amplified using colony PCR, employing the *E. coli* MG1655 strain as a template and appropriate primer, as listed in Supplementary Table 2. The plasmids pTΔptsG, pTΔcrr, pTΔpheA, pTΔsgrS, and pTΔpgi were used to delete *ptsG*, *crr*, *pheA*, *sgrS*, and *pgi*, respectively. The plasmid pTtrpE::tyrfbr was used to insert $tyrA^{fbr}$ in the *trpE* gene loci and pT*ptsG*::*galP-glk* to insert *galP-glk* in the *ptsG* gene loci.

Transformation of *E. coli* strains

Escherichia coli strains were transformed using electroporation with a 1350 kV, 600 Ω, and 10 μF electric pulse in a 0.1-cm cuvette using a Gene Pulser (Bio-Rad Laboratories, Hercules, CA, USA).

Analytical methods

Cell growth was analyzed by measuring OD_{600} using an UVmini-1240 spectrophotometer (Shimadzu Corporation, Kyoto, Japan). Glucose, xylose and fructose levels were measured using a Prominence high-performance liquid chromatography (HPLC) system (Shimadzu Corporation) equipped with a Shodex SUGAR KS-801 column (grain diameter, 6 μm; L × I.D., 300 × 8.0 mm; Showa Denko, Tokyo, Japan). Water was used as the mobile phase with a flow rate of 0.8 mL min^{-1} and the column was maintained at 50°C. The HPLC profile was monitored using a refractive index detector.

L-phenylalanine and L-tyrosine were analyzed using an HPLC system equipped with a PBr column (grain diameter, 5 μm; L × I.D., 250 × 4.6 mm; Nacalai Tesque, Inc., Kyoto, Japan). A dual-solvent system was used, in which solvent A was 0.2% phosphate buffer and solvent B methanol. The mobile phase flow rate was 1.0 mL min^{-1} and the column was maintained at 40°C. A gradient was initiated with an 80:20 mixture of solvents A and B (0–15 min), replaced by a 50:50 mixture of solvents A and B (15–20 min), and subsequently by an 80:20 mixture of solvents A and B (20–25 min). The HPLC profile was monitored using an ultraviolet-visible (UV-Vis) detector at a wavelength of 240 nm.

PEP, pyruvate, acetyl coenzyme A (CoA), G6P, F6P, F16BP, 6PG, Ru5P, Ro5P, E4P, S7P and 3PG + 2PG were analyzed using liquid chromatography–mass spectrometry (LC–MS), as detailed in the Metabolome analysis section.

Metabolome analysis

Metabolome analysis was conducted as previously reported with some modifications (Shirai *et al.*, 2013). Briefly, cells were cultured in M9Y medium supplemented with 20 g L^{-1} glucose until a mid-logarithmic growth phase was reached, corresponding to 18 h for EΔHI0, BPΔHI1, EΔHIG0 and BPΔHIG1. Afterwards, culture broth was harvested via rapid filtration. Filtered cells were dropped into cold methanol to rapidly quench metabolic flow and their intracellular metabolites were extracted in a 2.5:2.5:1 (v/v/v) $CHCl_3$:CH_3OH:H_2O mixture. Following centrifugation at 15,000 × g at 4°C for 15 min, the upper phase was collected. Metabolites were quantified by HPLC coupled with an electrospray ionization tandem mass spectrometry (LCMS-8040 triple quadrupole LC/MS/MS spectrometer; Shimadzu Corporation), using the Method Package for Primary Metabolites.

Measurement of BGL enzymatic activity

Each strain was cultured in LB medium at 37°C for 24 h. The periplasmic activity of BGL was evaluated using *p*-nitrophenyl-β-D-glucopyranoside (pNPG; Nacalai Tesque) as a substrate. One unit of BGL activity was defined as the amount of enzyme that produced 1 μmol min^{-1} of p-nitrophenol at 37°C and pH 5.0. The amount of p-nitrophenol produced was determined using a Synergy H1 microplate reader (BioTek Japan, Tokyo, Japan) at a wavelength of 400 nm. Apparent inhibition constants were calculated by curve-fitting the experimental values to the Morrison equation (Eq. 1) (Morrison, 1969).

$$\frac{v_i}{v_0} = 1 - \frac{\left([E] + [I] + K_{i-app}\right) - \sqrt{\left([E] + [I] + K_{i-app}\right)^2 - 4[E][I]}}{2[E]} \quad \text{(Eq. 1)}$$

[E], enzyme concentration; [I], inhibitor concentration; Ki-app, apparent inhibition constant; v0, initial rate observed in the absence of the inhibitor; vi, initial rate observed in the presence of the inhibitor.

Immunoblotting

Each strain was cultured at 37°C for 24 h in a modified M9 medium supplemented with glucose. The cells were subsequently centrifuged at 12,000 ×g at 4°C for 5 min, washed and resuspended in 500 µL of phosphate-buffered saline at pH 7. Afterwards, they were disrupted using a Micro Smash MS-100R (Tomy Seiko, Tokyo, Japan). Sodium dodecyl sulfate-polyacrylamide gel electrophoresis (SDS-PAGE) buffer (2% SDS, 10% glycerol, 5% 2-mercaptoethanol, 0.002% bromophenol blue, 0.125 M Tris-HCl; pH 6.8) was added to the supernatant, followed by boiling at 95°C for 5 min. Proteins were analyzed by SDS-PAGE using an e-PAGEL (Atto, Tokyo, Japan), including dual-color prestained Precision Plus protein standards (Bio-Rad Laboratories, Richmond, CA, USA) to serve as molecular weight markers. Proteins were electroblotted with an Amersham Hybond-P system (GE Healthcare, IL, USA) and incubated with an ANTI-FLAG M2 monoclonal antibody (Sigma-Aldrich, MO, USA) followed by an anti-rabbit IgG (Fc) AP conjugate (Promega Corp., Madison, WI, USA). Relative expression levels were calculated using NIH ImageJ v.1.8.0 software (http://rsbweb.nih.govij).

Measurement of surface plasmon resonance

The interaction between BGL and the glucose or G6P analytes was determined by SPR spectroscopy (Biacore T200; GE Healthcare). β-glucosidase was immobilized on a CM5 sensor chip with up to 8000 resonance units using 10 mM sodium acetate buffer (pH 4.2) containing 160 μg mL^{-1} BGL, delivered at a flow rate of 5 μL min^{-1} at 25°C. The running buffer was phosphate-buffered saline containing 0.005% Tween-20 and the analytes (glucose or G6P) were injected for 300 s at concentrations of 391–200 mM.

Quantification of mRNA transcription levels using real time PCR

The transcriptional expression of *uhpT* was quantified in each strain using real time PCR. Briefly, total RNA was isolated from individual cultures using a NucleoSpin RNA column (Takara Bio) according to the manufacturer's instructions. Reverse transcription and quantitative real time PCR were then performed using an Mx3005P real time QPCR system (Agilent Technologies, Santa Clara, CA, USA) with an RNA-direct SYBR green real time PCR master mix (Toyobo). Supplementary Table 2 lists the primer pairs. The normalized transcriptional level of each mRNA was lastly calculated and compared with the housekeeping gene *mdoG* (encoding glucan biosynthesis protein G) (Heng *et al.*, 2011).

Jar fermenter cultivation

Batch scale cultures were performed in 1.0 L jar fermenters with a 400 mL working volume at 37°C. For Phe production at this scale, we used the medium containing 3.29 g L^{-1} NaCl, 1.64 g L^{-1} KCl, 10 g L^{-1} $(NH_4)_2SO_4$, 10 g L^{-1} $MgCl_2 \cdot 6H_2O$, 14.7 mg L^{-1}

243 $CaCl_2$•$2H_2O$, 2.78 mg L^{-1} $FeSO_4$•$7H_2O$, 10 mg L^{-1} thiamine hydrochloride, 20 g L^{-1}
244 yeast extract, 50 g L^{-1} glucose, 100 mg L^{-1} L-tyrosine, 100 mg L^{-1} L-tryptophan, and 100
245 mg L^{-1} ampicillin. The medium (400 mL) in the jar fermenter was inoculated with
246 preculture medium to an initial OD_{600} of 0.03. DO was maintained at 2.04 p.p.m. by
247 automatically controlling the agitation speed from 200 to 800 r.p.m and supplementing
248 with air at 0.40 L min^{-1}. The pH was maintained above 6.8 with the automatic addition of
249 10% ammonia solution.

Results

BGL expression in the *E. coli* periplasm increases Phe production

The periplasmic expression of BGL is often employed in bioproduction, with cellobiose or cello-oligosaccharide as carbon sources (Georgiou and Segatori, 2005; Kurumbang et al., 2020; Nonaka et al., 2021; Satowa et al., 2020; Tanaka et al., 2011). Serendipitously, we found that periplasmic BGL expression altered the Phe production titer when glucose was used as a carbon source, even though glucose is not a BGL substrate. We thus focused on investigating how periplasmic expression of BGL affects Phe production.

We derived BGL from the *T. fusca* YX's Tfu0937 protein (UniProt Q47RE2), which exhibits enzymatic activity in *E. coli* (Soma et al., 2012; Tanaka et al., 2011). To induce periplasmic localization of Tfu0937, we used cell surface display, which anchors a target protein to the outer cell membrane, and signal sequence-mediated transport strategies. The C-terminus of the anchor protein Blc (UniProt P0A901), a lipoprotein localized to the outer cell membrane that is exposed to the periplasm, was fused to the N-terminus of Tfu0937, resulting in the periplasmic localization of Tfu0937 (Tanaka et al., 2011). Alternatively, the PelB signal peptide corresponding to the first 22 residues of pectate lyase B from *Erwinia carotovora* (UniProt P0C1C1) (Choi and Lee, 2004) was fused to the N-terminus of Tfu0937, thereby facilitating its transport to the periplasm without anchoring.

Phenylalanine-overproducing *E. coli* strain ATCC31882 was used as the parent strain for Phe production (https://www.atcc.org/products/all/31882.aspx, ATCC). We constructed four strains (named BD1, BP1, BC1, and E0). The E0 strain, harboring a high-copy

empty vector, was used as control. Strain BD1 harbored a high-copy plasmid expressing Tfu0937 fused with Blc (B-Tfu), strain BP1 harbored a high-copy plasmid expressing Tfu0937 fused with the PelB signal peptide (P-Tfu), and strain BC1 harbored a high-copy plasmid expressing intact Tfu0937, which is localized in the cytoplasm. After 48 h of cultivation using glucose as a substrate, BD1 and BP1 produced 1.46 ± 0.05 and 2.19 ± 0.10 g/L of Phe, respectively, which were 1.49- and 2.23 times higher than E0 (control strain; 0.98 ± 0.03 g L^{-1}), respectively (Fig. 1A). By contrast, compared with E0, BC1 produced 1.04 ± 0.21 g L^{-1} of Phe. There was no significant difference in cell growth (OD_{600}) of these four strains after 48 h of culture (Fig. S1A). Figure S1B shows specific BGL activity per cell density. There was no significant difference in specific BGL activity per cell density of BD1, BP1, and BC1. We confirmed Tfu0937 in strains by immunoblotting. Whole-cell extracts from BC1, BD1, and BP1 exhibited Tfu0937, B-Tfu, and P-Tfu expressions, respectively, at comparable levels (Fig. 1B). As described in a previous report, we observed in B-Tfu-expressing BD1 a band corresponding to the mass of unfused Tfu0937 (Ikeda et al., 2013). B-Tfu and P-Tfu were detected in periplasmic extracts of BD1 and BP1, respectively, at levels comparable to those in whole-cell extracts. However, Tfu0937 in the BC1 periplasmic extract was significantly decreased compared with that in the whole-cell extract (Fig. 1B). These results suggested that BGL localization to the periplasm positively affected Phe production, regardless of the localization method.

Next, we investigated how changing the number of plasmid copies would affect the Phe production. We constructed low- and medium-copy number plasmids for B-Tfu

296 expression that were introduced into ATCC31882, generating the strains BD1L (the low-
297 copy plasmid) and BD1M (the medium-copy plasmid). We used the strains E0L and
298 E0M, containing low- and medium-copy empty plasmids, respectively, as controls.
299 Figure 1C shows the relative amount of Phe produced from glucose in strains with
300 different copy numbers of plasmids. Phenylalanine production was increased 1.21, 1.39
301 and 1.48 times in strains BD1L, BD1M and BD1 (high-copy), respectively. We
302 confirmed a positive correlation between the copy number and BGL activity or
303 expression (Fig. 1D, S1C), indicating that Phe production and the B-Tfu expression
304 levels exhibit a positive, not directly proportional correlation. We confirmed the
305 correlation between BGL activity and Phe production. Based on these results, we used a
306 high-copy plasmid as the expression vector in the following experiments. We constructed
307 a strain, referred to as BD2, expressing an inactivated mutant BGL ($Tfu0937^{E388A}$) fused
308 with Blc ($B\text{-}Tfu^{E388A}$). As Glu388 is a putative nucleophilic residue required for
309 enzymatic activity in Tfu0937, the Glu388Ala mutant ($Tfu0937^{E388A}$) is rendered inactive
310 (Chir et al., 2011; Spiridonov and Wilson, 2001). Although the BD2 strain showed no
311 BGL activity (Fig. S1C), expectedly, it produced 1.86 g L^{-1} ± 0.07 g L^{-1} Phe from
312 glucose, which was 1.90 times higher than the control strain (E0) (Fig. S1D). The
313 periplasmic localization of inactivated BGL also had a positive effect on Phe production,
314 indicating that BGL enzymatic activity was not required to increase Phe production.
315 Thus, we suspected that an unknown mechanism could underlie the increased Phe
316 production driven by periplasmic BGL localization.
317

Periplasmic BGL localization does not affect Phe production in EIIC^{Glc} domain-deficient strains

The phosphotransferase (PTS) system simultaneously mediates sugar transport and phosphorylation (Fig. 2A). Glucose uptake in *E. coli* involving the PTS system comprises four proteins located in either the inner membrane or cytoplasm: enzyme I (EI, encoded by *ptsI*), HPr (encoded by *ptsH*), enzyme IIA (EIIA, encoded by *crr*) and EIICB^{Glc} (encoded by *ptsG*). The enzymes EI, HPr and EIIA are cytoplasmic, whereas EIICB^{Glc} is a transmembrane protein with two domains: an N-terminal membrane-spanning EIIC^{Glc} domain containing a carbohydrate-binding site and a C-terminal cytoplasmic EIIB^{Glc} domain containing a phosphorylation site (Cys421). EI and HPr are involved in the transport of numerous sugars, whereas EIIA, EIIB and EIIC are sugar-specific. In the PTS system, 1 mol PEP is converted to 1 mol pyruvate during the transport of 1 mol glucose into the cell. The phosphate group of PEP is transferred to the EI, then relayed to the HPr and EIIB domains. Glucose is subsequently transported from the periplasm to the cytoplasm via the EIIC^{Glc} domain of EIICB^{Glc} and simultaneously converted to G6P via phosphoryl transfer from the phosphorylated EIIB^{Glc} domain. Although the PTS system is the main glucose transport system in bacteria, *E. coli* also uses the galactose permease/glucokinase (GalP/Glk) system (Fig. 2A). The GalP is a galactose permease with 12 transmembrane α helices (Zheng et al., 2010) involved in the transport of galactose, its main substrate, and glucose. Its expression is repressed when *E. coli* is grown in the presence of glucose (Hernández-Montalvo et al., 2003). The Glk, a glucokinase, localizes to the cytoplasm where it catalyzes ATP-dependent glucose phosphorylation (Hernández-Montalvo et al., 2003).

The PTS system is a major metabolic reaction that competes with the shikimate pathway for PEP consumption (Fujiwara et al., 2020). Replacing the PTS system with another sugar-specific transport system, such as the GalP/Glk system, is often employed to increase the amount of PEP available for the shikimate pathway (Hernández-Montalvo et al., 2003). Previously, we constructed an ATCC31882-derived strain named CFT1, in which two PTS-related genes, *ptsI* and *ptsH*, were replaced with the GalP/Glk system (Noda et al., 2016). To investigate the effects of periplasmic BGL localization in our metabolically engineered system, we evaluated Phe production using the CFT1 strain. The BDΔHI1 (CFT1 expressing B-Tfu) and BPΔHI1 (CFT1 expressing P-Tfu) strains produced 3.51 ± 0.10 and 3.44 ± 0.12 g/L Phe (Fig. 2B), which were 1.30- and 1.27 times higher, respectively, than the EΔHI0 strain (CFT1 harboring an empty vector) (2.70 ± 0.24 g L^{-1} Phe). Using glucose as the sole carbon source in BPΔHI1 strains, the Phe yields was 0.24 mol mol^{-1} close to the highest values reported previously (0.26 mol mol^{-1} in a fed-batch culture, 0.23 mol mol^{-1} in batch culture) (Zhou et al., 2010). In BDΔHI1 and BPΔHI1 strains, intracellular PEP increased by 1.2 and 2.6 times, respectively, compared to the EΔHI0 strain (Fig. S2A, B). Contrastingly, intracellular pyruvate and acetyl-CoA levels were decreased in BDΔHI1 and BPΔHI1 strains compared to the EΔHI0 strain (Fig. S2A, B). This finding suggested that periplasmic BGL localization increased PEP accumulation in *ptsHI*-deficient strains, an effect that was most pronounced in BPΔHI1. We thus used the PelB signal peptide to drive periplasmic protein localization in subsequent experiments.

363 Considering that EI and HPr (lacking in the strain CFT1) are localized in the cytoplasm,
364 we suspected that these proteins are not involved in this phenomenon. To determine the
365 contribution of other PTS proteins in improving Phe production, we constructed strains
366 that disrupted other PTS proteins *crr* or *ptsG*, which encode EIIA (cytoplasm) and
367 $EIICB^{Glc}$ (transmembrane), respectively, in CFT1 strain. We named the resultant strains
368 CFT1Δ*crr* and CFT1Δ*ptsG*. We cultured BPΔHIC1 (CFT1Δ*crr* expressing P-Tfu),
369 EΔHIC0 (CFT1Δ*crr* harboring an empty vector), BPΔHIG1 (CFT1Δ*ptsG* expressing P-
370 Tfu), and EΔHIG0 (CFT1Δ*ptsG* harboring an empty vector) in a medium containing
371 glucose as the sole carbon source. The BPΔHIC1 strain produced 3.00 ± 0.19 g L^{-1} of
372 Phe, 1.57 times higher than that produced by the EΔHIC0 strain (1.91 ± 0.13 g L^{-1}; Fig
373 2C). By contrast, BPΔHIG1 produced a similar amount of Phe (2.34 ± 0.12 g L^{-1}) as
374 EΔHIG0 (2.39 ± 0.25 g L^{-1}; Fig. 2C), indicating that *ptsG* was required for periplasmic
375 BGL localization to facilitate increased Phe production in the CFT1-derived strain.
376 BPΔHIG1 exhibited a significant decrease in intracellular PEP compared with the
377 EΔHIG0 control (Fig. S2C), contrary to the effect observed between BPΔHI1 and EΔHI0
378 shown in Figure S2B. We found no significant differences in intracellular pyruvate and
379 acetyl-CoA levels between EΔHIG0 and BPΔHIG1 (Fig. S2C), which also differed from
380 the result shown in Figure S2B. Cumulatively, these results indicate that *ptsG* is a key
381 factor mediating the BGL-dependent increase in Phe production.
382
383 To further elucidate the effects of *ptsG* disruption, we constructed the strain disrupting
384 *ptsG* in the ATCC31882 background and named it ATCC31882Δ*ptsG*. We cultured
385 BPΔG1 (ATCC31882Δ*ptsG* expressing P-Tfu) and EΔG0 (ATCC31882Δ*ptsG* harboring

386 an empty vector) using glucose as the sole carbon source. Consistent with our previous
387 results, the EΔG0 and BPΔG1 strains produced 1.57 ± 0.06 and 1.54 ± 0.09 g $L^{-1}$of Phe,
388 respectively, with no significant difference (Fig. 2D). We found no significant differences
389 in intracellular PEP, pyruvate, and acetyl-CoA levels between EΔG0 and BPΔG1
390 (Fig. S2D). These results strongly support that *ptsG* is a key factor in this phenomenon.
391 We constructed an ATCC31882 strain containing the endogenous $EIICB^{Glc}$ protein
392 inactivated via point mutation and named it C421S. During glucose transport, $EIICB^{Glc}$
393 receives a phosphate group from EIIA on Cys421, which allows it to serve as a phosphate
394 group donor for glucose; therefore, we eliminated the phosphorylation capability of
395 $EIICB^{Glc}$ by creating the Cys421Ser mutant. The strain $BP^{C421S}1$ (C421S expressing P-
396 Tfu) produced 2.03 ± 0.03 g L^{-1} of Phe, 1.36 times higher than that produced by $E^{C421S}0$
397 (C421S harboring an empty vector) (Fig. 2D). These results indicate that although
398 $EIICB^{Glc}$ presence is required for periplasmic BGL-dependent Phe production,
399 phosphorylation of Cys421 is unnecessary. To investigate specific roles of the $EIIB^{Glc}$
400 and $EIIC^{Glc}$ domains in this phenomenon, we constructed two strains derived from
401 ATCC31882Δ*ptsG*—strain dGB (ATCC31882Δ*ptsG* harboring pZA23-$EIIB^{Glc}$)
402 expressed only the $EIIB^{Glc}$ domain, strain dGC (ATCC31882Δ*ptsG* harboring pZA23-
403 $EIIC^{Glc}$) expressed only the $EIIC^{Glc}$ domain. Strains EdGB0 (dGB harboring an empty
404 vector) and BPdGB1 (dGB expressing P-Tfu), which express only the $EIIB^{Glc}$ domain,
405 produced Phe with insignificant difference in production (Fig. 2E). By contrast, strains
406 EdGC0 (dGC harboring an empty vector) and BPdGC1 (dGC expressing P-Tfu), which
407 express only the $EIIC^{Glc}$ domain, produced 0.73 ± 0.03 and 1.85 ± 0.07 g L^{-1} of Phe,
408 respectively, and the titer in BPdGC1 was 2.5 times higher than that in the EdGC0

409 control (Fig. 2E). These results demonstrate that the EIIC^{Glc} domain is specifically
410 necessary for the periplasmic BGL-dependent increase in Phe production, unlike the
411 EIIB^{Glc} domain.
412
413 **G6P—a key metabolite, as demonstrated via metabolome analysis**
414 Our results indicate that EIICB^{Glc}, encoded by *ptsG*, is a key factor in increasing Phe
415 production. However, the direct interaction between B-Tfu and the EIIC^{Glc} domain is
416 likely impossible because B-Tfu is anchored at the cell's outer membrane, whereas
417 EIIC^{Glc} domain is present on the cell's inner membrane. Therefore, we hypothesized that
418 EIIC^{Glc} domain could act as a transporter for another key metabolite that would interact
419 with B-Tfu in the periplasmic space.
420
421 To identify metabolites involved in periplasmic BGL-dependent Phe production, we
422 cultured EΔHI0 and the strain expressing P-Tfu derived from CFT1 (BPΔHI1) using
423 glucose as a substrate and measured the intracellular concentration (including cytosol and
424 periplasm) of glycolysis and pentose phosphate pathway (PPP) metabolites (Fig. 3A, B).
425 Although intracellular levels of 6-phosphogluconate and erythrose-4-phosphate were
426 slightly decreased in BPΔHI1 compared with EΔHI0, most other glycolysis and pentose
427 phosphate pathway (PPP) metabolites were also not significantly different between the
428 strains or were decreased in BPΔHI1 (Fig. 3B). Interestingly, intracellular G6P
429 concentration was increased by 2.25 times in BPΔHI1 compared with that in EΔHI0 (Fig.
430 3B). Moreover, we found no significant differences in the G6P concentration between
431 EΔHIG0 and BPΔHIG1 (CFT1Δ*ptsG* expressing P-Tfu) (Fig. S3A).

Metabolome analysis suggested that G6P was a candidate metabolite potentially involved in improving periplasmic BGL-mediated Phe production. To confirm this, we examined Phe production using non-G6P sugars (xylose or fructose) as carbon sources. In the *E. coli* catabolic pathway, glucose entering the cell through the PTS or GalP/Glk systems is converted to G6P to initiate glycolysis. Both G6P and F6P are readily interconverted by G6P isomerase. Xylose is transported into the cell by xylose-specific ATP-binding cassette transporters or the xylose-proton symporter and converted to xylulose, which is subsequently converted to xylulose-5-phosphate entering PPP. Fructose is further transported by the fructose-specific PTS and converted to fructose-1-phosphate (F1P), which, in turn, is converted to F16BP entering glycolysis (Fig. S3B). When xylose or fructose are used as a carbon source, carbon flows into G6P and F6P in low proportions due to its utilization via PPP or gluconeogenesis. Therefore, the xylose and fructose used as a carbon source are catabolized with less conversion to G6P, reducing the intracellular G6P concentration. When xylose or fructose were used as carbon source, BP ΔHI1 produced 0.49 ± 0.02 and 0.21 ± 0.06 g L^{-1} of Phe (Fig. S3C), respectively, which is comparable to the amounts produced by the control (EΔHI0) (0.52 ± 0.05 and 0.21 ± 0.02 g L^{-1}, respectively). The intracellular G6P concentrations did not significantly differ between BPΔHI1 and EΔHI0 (Fig. S3D, E). This observation suggested that G6P is a key metabolite in the periplasmic BGL localization as proposed (Fig. 3C).

For G6P to act as a key metabolite, its interaction with BGL is required. We measured the fractional enzymatic activity of BGL in the presence of excess G6P or glucose and found

that it decreased more in response to G6P compared with excess glucose. The apparent inhibition constants were 595 and 295 mM for glucose and G6P, respectively (Fig. 3D). This finding indicated that Tfu0937 has a higher affinity for G6P than glucose, although Tfu0937 has no catalytic activity against G6P. We used surface plasmon resonance to measure the interaction between BGL and glucose or G6P. The sensorgrams indicate that although BGL interacts with both metabolites, it exhibits a higher affinity for G6P than glucose (Fig. 3E). These results support our hypothesis that BGL interacts with G6P in the periplasm.

G6P secretion and accumulation in the periplasm

Metabolome analysis revealed that intracellular G6P levels, comprising both cytoplasmic and periplasmic fractions, increased significantly with periplasmic BGL localization. To ensure that the $EIIC^{Glc}$ domain functions as a cytoplasm-to-periplasm G6P transporter, quantifying G6P levels in the periplasm exclusively would be required. However, we were unable to quantify the periplasmic G6P, while excluding cytoplasmic content. We thus measured the messenger RNA (mRNA) of *uhpT* as a strong indicator of periplasmic G6P concentration. Expression of the hexose phosphate transporter (UhpT) is strictly controlled by the UhpABC regulatory system (also named the Uhp system, Fig. 4A). A non-linear positive correlation also exists between the induction of *uhpT* transcription and G6P concentration in the medium (Västermark and Saier, 2014; Verhamme et al., 2002, 2001). When UhpC senses periplasmic G6P, the UhpBC complex changes conformation, leading to the autophosphorylation of UhpB (P-UhpB) using ATP as the phosphoryl group donor(Västermark and Saier, 2014). The phosphoryl group of P-UhpB is then

transferred to UhpA, which binds to the transcriptional regulatory promoter region of *uhpT*, enhancing *uhpT* transcription (Västermark and Saier, 2014; Verhamme et al., 2002, 2001). We determined whether the presence of G6P in the medium increased *uhpT* transcription levels, as previously reported (Verhamme et al., 2002). We observed a non-linear positive correlation between *uhpT* transcription levels in ATCC31882 and the quantity of G6P supplemented in the medium (Fig. 4B). Therefore, we were able to successfully use *uhpT* transcription level to measure periplasmic G6P concentration.

We cultured E0, EΔG0, and $E^{C421S}0$ strains using glucose as the carbon source and measured the *uhpT* transcription levels. Figure 4C shows the relative *uhpT* transcription levels in strains E0, EΔG0, and $E^{C421S}0$. The *uhpT* transcription in EΔG0 was significantly lower than that in the control (E0), whereas the *uhpT* transcription in $E^{C421S}0$ was comparable to that in E0. Considering that $E^{C421S}0$ expressed a variant $EIICB^{Glc}$ protein with an inactivated phosphate donor domain ($EIIB^{Glc}$ domain) and native membrane-spanning domain ($EIIC^{Glc}$ domain), these results support our hypothesis that the $EIIC^{Glc}$ domain acts as a G6P transporter regardless of whether the EIIB domain exhibits phosphorylation activity.

Second, we investigated how the periplasmic BGL localization affects the periplasmic G6P concentration. The *uhpT* expression levels were compared in the glucose-containing medium between E0 and BP1 or between EΔG0 and BPΔG1. BP1 exhibited significantly higher *uhpT* levels compared with the control (E0), suggesting that periplasmic BGL localization causes periplasmic G6P accumulation (Fig.4D). Alternatively, the *uhpT*

levels were comparable between EΔG0 and BPΔG1 (Fig. 4E), suggesting that *uhpT* transcription was not activated by the periplasmic localization of BGL when EIICB^{Glc} was absent and incapable of secreting G6P into the periplasm (Fig. 4C, E).

To investigate further G6P transport via the EIIC^{Glc} domain, we constructed another ATCC31882-derived EIICB^{Glc}-deficient strain, named P2Gs. In the P2Gs strain, *ptsG* was replaced by the *galP-glk* operon and disrupted *sgrS* which encodes a small RNA triggering the degradation of *ptsG* mRNA that can be activated by the accumulation of intracellular G6P (Poddar et al., 2021). This *sgrS* disruption prevented the unintended mRNA degradation when EIIC^{Glc} was overexpressed. We constructed two strains, P2GsE (P2Gs harboring an empty vector) and P2GsC (P2Gs harboring pZA23-EIIC^{Glc}), and cultured them with glucose as a carbon source. The intracellular G6P concentration (including the cytoplasmic- and the periplasmic-G6P) and *uhpT* expression levels were compared between P2GsE and P2GsC in the logarithmic phase (7 h after cultivation). No significant difference could be observed in the intracellular G6P levels between P2GsE and P2GsC (Fig. 4F). This result indicated that the presence or absence of EIIC^{Glc} does not affect the total amount of intracellular G6P. However, *uhpT* expression in P2GsC was 2.82 times higher than in P2GsE (Fig. 4F). This result indicated that overexpressing the EIIC^{Glc} domain increased periplasmic G6P concentration, by transporting G6P from the cytoplasm to the periplasm. We constructed a G6P-accumulating strain by disrupting *pgi* from P2Gs, named P2GsΔ*pgi*, and confirmed an increase in *uhpT* expression resulting from increased G6P secretion. The strain P2GsCΔ*pgi* (P2GsΔ*pgi* harboring pZA23-EIIC^{Glc}) was cultured with glucose as a carbon source. The intracellular G6P

concentration in the P2GsCΔ*pgi* strain increased 4.34 times compared to the P2GsC strain, while *uhpT* expression in the P2GsCΔ*pgi* strain was 6.23 times higher than in the P2GsC strain. These results support further our hypothesis that the $EIIC^{Glc}$ domain transports cytoplasmic G6P into the periplasm.

We also investigated the *uhpT* levels in the glucose-containing medium between EΔHI0 and BPΔHI1. The *uhpT* level was 4.18-times higher in BPΔHI1 than in EΔHI0 (Fig. 4G). In BPΔHI1, the intracellular G6P (including the cytoplasmic- and the periplasmic-G6P) also increased compared with that in EΔHI0 (Fig. 3B). Taken together, these results suggest that the BGL-related G6P capture in the periplasm increased the periplasmic G6P concentration, resulting in an increased total amount of intracellular G6P.

Next, we confirmed the effect of the periplasmic G6P, supplied from outside the cell, on Phe production. We cultured strain E0 with G6P as a sole carbon source instead of glucose. Cell growth and Phe production in E0 were at the same levels using G6P as a carbon source or glucose (Fig. S4A, B). Since direct G6P supplementation to the medium did not improve Phe production, we considered the increased periplasmic G6P concentration insufficient to increase Phe production. To clarify the necessary requirements for this phenomenon to activate Phe production, we examined Phe production in strains localizing BGL to the periplasm, BP1 and BPΔG1, with G6P as a carbon source. The BP1 strain produced 1.3 times higher levels of Phe than the control strain E0 (0.93 ± 0.01 and 0.70 ± 0.02 g L^{-1}, respectively; Fig. S4C). However, no significant difference could be observed between BPΔG1 and the control strain EΔG0

(0.47 ± 0.04 and 0.42 ± 0.01 g L^{-1}, respectively; Fig. S4D). This result suggests that the interaction between G6P and BGL is an important factor in increasing Phe production. In addition, it was suggested that the secretion of G6P into the periplasm via the $EIIC^{Glc}$ domain is necessary to increase Phe production even when G6P is sufficiently supplemented in the periplasm from the medium.

Application of other proteins using the proposed mechanism

As we have previously described, the $EIIC^{Glc}$ domain and G6P are key factors for improving Phe production. Our current and previous results on G6P support a leading hypothesis that G6P is transported from the cytoplasm to the periplasm via the $EIIC^{Glc}$ domain and accumulates in the periplasm, where G6P-capturing proteins including BGL localize (Fig. 5A). Based on this mechanism, we assumed that the periplasmic localization of other enzymes with an affinity for G6P would also positively affect Phe production.

We selected three enzymes, G6P isomerase (Pgi), encoded by *pgi*; G6P 1-dehydrogenase (Zwf), encoded by *zwf*; and alkaline phosphatase (PhoA), encoded by *phoA*, and their inactivated mutants as candidates. To facilitate their periplasmic localization, we fused Pgi, Zwf, Pgi^{H386A} (inactivated form), and Zwf^{H239A} (inactivated form) with the PelB signal peptide and named them PelB-Pgi, PelB-Zwf, PelB-Pgi^{H386A}, and PelB-Zwf^{H239A}, respectively. PhoA is a native periplasmic enzyme (Chung Nan Chang et al., 1986). Using ATCC31882, we constructed eight strains localizing these proteins to the cytoplasm or periplasm: PC1 (expressing Pgi), ZC1 (expressing Zwf), PP1 (expressing

570 PelB-Pgi), ZP1 (expressing PelB-Zwf), AP1 (expressing PhoA), PP2 (expressing PelB-
571 Pgi^{H386A}), ZP2 (expressing PelB-Zwf^{H239A}), and AP2 (expressing $PhoA^{S124A}$, inactivated
572 form). In addition, we constructed a strain expressing green fluorescent protein (GFP), a
573 non-enzymatic protein, in the periplasmic space as a control and called this GP1.
574
575 Because Pgi and Zwf are enzymes involved in glycolysis and PPP, we first examined
576 how overexpressing these enzymes in the cytoplasm affects Phe production. There was
577 no significant difference in Phe production observed between PC1 and E0 (control
578 strain), whereas the strain ZC1 resulted in 1.6 times higher Phe production compared to
579 E0 (Fig. S5A). The Zwf enzyme catalyzes the first reaction of PPP. Because erythrose 4-
580 phosphate, a PPP intermediate, is another starting metabolite for the shikimate pathway,
581 Zwf overexpression might have increased carbon flux into PPP, thereby enhancing the
582 shikimate pathway.
583
584 Figure 5B shows the results for Phe production in the strains PP1, ZP1, AP1, PP2, ZP2,
585 and AP2. The control strain GP1 produced 0.74 ± 0.03 g L^{-1}, whereas strains PP1, ZP1,
586 and AP1 produced 0.62 ± 0.01, 0.99 ± 0.14, and 1.16 ± 0.19 g L^{-1} of Phe, respectively.
587 PP1 produced lesser Phe than the control (E0), and we found no significant difference in
588 Phe production between ZP1 and E0 and between AP1 and E0. Although Zwf
589 overexpression in the cytoplasm in strain ZC1 increased Phe production, the strain ZP1,
590 which overexpresses Zwf in the periplasm, produced the same level of Phe as E0.
591 Contrastingly, strains PP2, ZP2, and AP2, which lacked an enzymatic activity, produced
592 1.69 ± 0.09, 1.43 ± 0.09, and 1.64 ± 0.09 g L^{-1} of Phe, respectively, which was

593 significantly higher than that produced by E0. Although Zwf expression in the periplasm
594 was similar between ZP1 and ZP2, only ZP2 exhibited increased Phe production
595 compared with E0 (Fig. S5B). These results suggest that the mechanism of increased Phe
596 production in ZP2 is not attributed to increased PPP. In the strains with periplasmic
597 localization of inactivated enzymes (PP2, ZP2, and AP2), the intracellular G6P levels
598 were significantly increased compared with E0 (Fig. S5C). These results suggest that the
599 periplasmic localization of proteins that have affinity for G6P but do not exhibit
600 enzymatic activity for it can facilitate increased Phe production, supporting the
601 hypothesized mechanism (Fig. 5A).
602
603 **Production of other metabolites using G6P-capturing proteins**
604 To demonstrate our method's ability to increase the production of other shikimate
605 pathway derivatives, we investigated Tyr and MA production using the strains that
606 localize G6P-capturing proteins in the periplasm (Fig. 6A). For Tyr production, we
607 constructed a CFT1-derived strain, named TYR, by disrupting *pheA* encoding chorismate
608 mutase/prephenate dehydratase and inserting *tyrA* into the *trpE* gene locus. We further
609 constructed two TYR-derived strains: TYR1 (expressing B-Tfu) and TYR0 (harboring an
610 empty vector). We cultured TYR1 and TYR0 using glucose as the carbon source. Strains
611 TYR0 and TYR1 produced 2.20 ± 0.03 and 2.73 ± 0.05 g L^{-1} of Tyr, respectively, while
612 Tyr production was 1.24 times higher in TYR1 compared to TYR0 (Fig. 6B). In the strain
613 TYR1, Tyr yield from glucose was 0.15 mol mol^{-1}. In the Tyr production, two bottleneck
614 reactions were identified in the shikimate pathway (Juminaga et al., 2012). In this study,
615 TYR1 strain was not modified to relieve those bottlenecks. However, the technique of

expressing G6P-capturing protein in the periplasm is compatible with traditional metabolic engineering techniques, such as relieving bottlenecks; thus, we believe that Tyr yield could be increased in TYR1-derived strains by optimizing the shikimate pathway.

For MA production, we selected the MA synthesis pathway that starts from 3-dehydroshikimate (DHS), a shikimate pathway intermediate. In this pathway, which has the highest theoretical yield among all MA synthetic pathways, DHS is converted to protocatechuate (PCA) by DHS dehydratase (*aroZ*), then PCA is converted to catechol (CA) by PCA decarboxylase (*aroY*), and finally CA is converted to MA by CA 1,2-dioxygenase (*catA*) (Fujiwara et al., 2020). We first constructed the CFT1Δ*pheA* strain derived from CFT1 by disrupting *pheA*, then the CFT1Δ*pheA*MA strain by introducing CFT1Δ*pheA* into the MA synthesis pathway. We also constructed two CFT1Δ*pheA*MA-derived strains: MA1 (expressing P-Tfu) and MA0 (harboring an empty vector). Finally, we cultured MA1 and MA0 using glucose as the carbon source. Strains MA1 and MA0 produced 2.50 ± 0.21 and 1.49 ± 0.03 g L^{-1} MA, respectively, while MA production was 1.68 times higher in MA1 than MA0 (Fig. 6C). In the strain MA1, MA yield from glucose was 0.15 mol mol^{-1}. Previously, we succeeded at producing high-yield MA (0.28 mol mol^{-1}) using metabolically engineered *E. coli* expressing fused enzymes (Fujiwara et al., 2018). These findings reveal that a combination of periplasmic G6P-capturing protein technique and existing technology has the potential of increasing MA yield beyond Tyr production.

638 Together, the results of the Tyr and MA production experiments indicate that the
639 periplasmic expression of G6P-capturing proteins can increase the production of
640 metabolites derived from chorismate, i.e., the end product of the shikimate pathway, and
641 from shikimate pathway intermediates.
642
643 **Phe production using a 1-L jar fermenter**
644 Batch cultures of EΔHI0 and BPΔHI1 were performed using a 1-L jar fermenter. The
645 modified M9 medium with 50 g L^{-1} of glucose was used. Figure 7 shows the EΔHI0 and
646 BPΔHI1 culture profiles in the jar fermenter. BPΔHI1 produced 6.32 g L^{-1} of Phe after
647 48 h of cultivation, which is 1.46 times higher than that produced by EΔHI0 (4.34 g L^{-1}).
648 In the BPΔHI1 strain, the Phe yield from glucose was 0.13 mol mol^{-1}, which is 1.41
649 times higher than that in EΔHI1, although it decreased compared to the test tube culture
650 of the BPΔHI1 strain (0.24 mol mol^{-1}). This result indicates that periplasmic GCP
651 localization leads to enhancement of the shikimate pathway even in the case of jar
652 fermenter cultivation. The Phe production yield in BPΔHI1 was lower than the highest
653 Phe production yield reported to date (0.26 mol mol^{-1} in a fed-batch culture, 0.23 mol
654 mol^{-1} in batch culture) (Zhou et al., 2010). Zhou et al. used the L-tyrosine auxotrophic
655 strain *E. coli* WSH-Z06, which is a laboratory strain of unknown genetic background, for
656 Phe production. Since the L-tyrosine and L-tryptophan auxotrophic strains were used for
657 Phe production in the present study, our strategy is likely applicable to the other strains
658 that produced high yield shikimate pathway derivatives reported in previous studies.

Discussion

We demonstrated that localization of G6P-capturing proteins, including BGL, in the periplasm of *E. coli* accelerates the shikimate pathway. Positive effects of this BGL periplasmic localization on Phe production were also observed in strains metabolically engineered using a traditional approach. Other proteins with affinity for G6P similarly exerted a positive effect on Phe production when they localized to the periplasm. This phenomenon further resulted in the production of other shikimate pathway derivatives, i.e., Tyr and MA.

To reveal the underlying mechanisms, we identified key factors involved in this phenomenon: the G6P-capturing protein, G6P, and $EIIC^{Glc}$ domain. Acceleration of the shikimate pathway was prevented with the absence of any one of these key factors. We confirmed the interaction between BGL and G6P by investigating enzymatic activity and SPR, as well as G6P secretion via the $EIIC^{Glc}$ domain by measuring *uhpT* expression. Based on the results, we propose that the $EIIC^{Glc}$ domain functions as a G6P transporter secreting G6P into the periplasm, while G6P dynamically binds to and detaches from G6P-capturing proteins in the periplasm. As intracellular PEP was increased by the periplasmic BGL localization, it was suggested that the accumulation of intracellular PEP accelerates the shikimate pathway. However, the mechanisms by which the proposed model causes intracellular PEP accumulation remain unclear.

Suppression of the PTS system has been used in many studies as a metabolic engineering approach to strengthen the shikimate pathway (Nakagawa et al., 2011; Noda and Kondo,

682 2017). The first step of the PTS system, the transfer of phosphate groups from PEP to EI,
683 is a major PEP consumption reaction that contributes to reducing carbon flux in the
684 shikimate pathway. A recent study reported a reverse reaction producing PEP from
685 pyruvate when a phosphate group was received from phosphorylated EI (Long et al.,
686 2017). Hence, the PTS system is deeply involved in regulating the balance between PEP
687 and pyruvate, two metabolic branch points. In the present study, the strain disrupting
688 *ptsHI*, encoding EI, had a positive effect on Phe production through periplasmic BGL
689 localization. This result implies that an acceleration of the shikimate pathway by the
690 periplasmic BGL localization is not due to PEP consumption suppression in the PTS
691 system. In addition, the intracellular PEP concentration was increased by periplasmic
692 BGL localization in the *ptsHI*-deficient strain, which indicates that the intracellular PEP
693 accumulation results from a mechanism other than suppressing PEP consumption by the
694 PTS system.
695
696 To transduce environmental information into appropriate cellular responses, the two-
697 component system (TCS) is widely used in organisms that include *E. coli* (Jacob-
698 Dubuisson et al., 2018). The TCS system comprises a sensor histidine kinase (SHK) and
699 a cognate cytoplasmic response regulator (Jacob-Dubuisson et al., 2018). The SHK
700 sensor domain is exposed to the periplasm and senses signals such as chemicals. When
701 the SHK sensor domain senses signals, the response regulator takes a phosphorylated
702 form through several steps. The phosphorylated response regulators can control the
703 cellular condition, such as metabolism, by functioning as DNA-binding transcription
704 factors. They can also display RNA-binding, protein-binding, or even enzymatic

activities (Jacob-Dubuisson et al., 2018). The Uhp system is a TCS that induces *uhpT* expression, encoding the hexose-6-phosphate:phosphate antiporter, by its periplasmic G6P (Västermark and Saier, 2014; Verhamme et al., 2002, 2001). In the present study, when using G6P as a carbon source instead of glucose, Phe production did not increase in the strain without G6P-capture proteins localization to the periplasm. This result suggested that increasing periplasmic G6P concentration is only insufficient to accelerate the shikimate pathway. In other words, the acceleration of the shikimate pathway does not result from the periplasmic G6P concentration by TCSs, including the Uhp system. In the G6P containing medium, periplasmic BGL localization increased Phe production in the strain where *ptsG* remained intact, which did not occur in a *ptsG*-deficient strain. This result suggested that G6P secretion from the cytoplasm into the periplasm via the $EIIC^{Glc}$ domain is essential for accelerating the shikimate pathway, even in the presence of high levels of periplasmic G6P. The ratio of cytoplasmic G6P concentration or G6P concentration between the periplasm and cytoplasm might contribute to this phenomenon.

The regulatory mechanisms of the cytoplasmic metabolism have been well studied and various applied techniques for bioproduction have been developed (Nielsen and Keasling, 2016). However, the mechanisms regulating the periplasmic environment remain largely unknown. Changes in the periplasmic environment, including those in the periplasmic G6P levels, can affect overall metabolism. In the present study, periplasmic GCP expression results in an increased intracellular G6P concentration (Fig. 3B and S5C). Fig. 4D shows that the *uhpT* expression level in BP1 was significantly higher than that in E0,

indicating that the periplasmic concentration of free G6P was increased due to periplasmic BGL expression. We demonstrated that the periplasmic localization of intact/inactivated BGL or the three kinds of GCPs increased the Phe production (Figs. 1 and 5). Further, we confirmed that when a protein with no G6P affinity (GFP) was localized in the periplasm, no positive effect was observed on the Phe production. Even when the periplasmic concentration of free G6P is the same, the total G6P concentration in the periplasm (including free G6P and GCP–G6P complex) is higher when GCP is present in the periplasm (Supplementary Discussion 1). However, when the dissociation constant between GCP and G6P (Kd) is comparable to the apparent inhibition constant (Ki, Fig. 3D), the contribution of G6P-GCP affinity to the increasing G6P concentration would be limited. These results suggest that the periplasmic expression of GCP activates unknown mechanisms that increase the amount of G6P secreted in the periplasm and/or decrease the amount of G6P reuptake in the cytoplasm.

A hypothesis that explains the phenomenon identified in this study is that changes in the periplasmic environment resulted in a change in the intracellular G6P level and its balance between the cytoplasm and periplasm, affecting the overall metabolism, resulting in PEP accumulation and the acceleration of the shikimate pathway. Further elucidation of the mechanism requires individual G6P concentration measurement both in the periplasm and the cytoplasm, but it is technically difficult at present, partially because it is difficult to separate the small molecules present in the periplasm from the whole cell components and their concentrations cannot be measured accurately.

Conclusions

Here, we successfully discovered a new phenomenon that is beneficial for bioproduction and identified three key factors involved in this phenomenon—the G6P-capturing protein, G6P, and $EIIC^{Glc}$ domain. Modification of the periplasmic environment via the expression of proteins having affinity for G6P is an original approach to increase target metabolite yield in bioproduction.

Acknowledgments

This work was supported by the JST-Mirai Program (Grant Number JPMJMI17EI), Japan (to S.N. and T.T.). Additionally, it was supported by the Japan Society for the Promotion of Science (JSPS) Grant-in-Aid for Scientific Research (B) (Grant Number 19H02526), Japan (to T.T.). R.F. received support from Research Fellowship for Young Scientists from JSPS. This work was supported by the RIKEN Center for Sustainable Resource Science, Special Postdoctoral Researcher Program (to S.N.). The authors would like to thank Enago (www.enago.jp) for the English language review.

Author contributions

Conceptualization, R.F., T. S., S.N., and T.T.; Methodology, R.F., T. S., S.N., and T.T.; Formal Analysis, R.F., T. S., S.N., and T.T.; Writing–Original Draft, R.F.; Writing–Review & Editing, S.N., and T.T.; Investigation, R.F., M.N., Y.H., C.O., D.N., S.N., T.T., S. K., H. N., and M. U.; Supervision, A.K.

Declaration of competing interest

Kobe University has filed a patent application related to this technology on behalf of R.F., S.N., and T.T. The patent application number is JP 2019-123262. Other authors declare no competing interests.

Figures

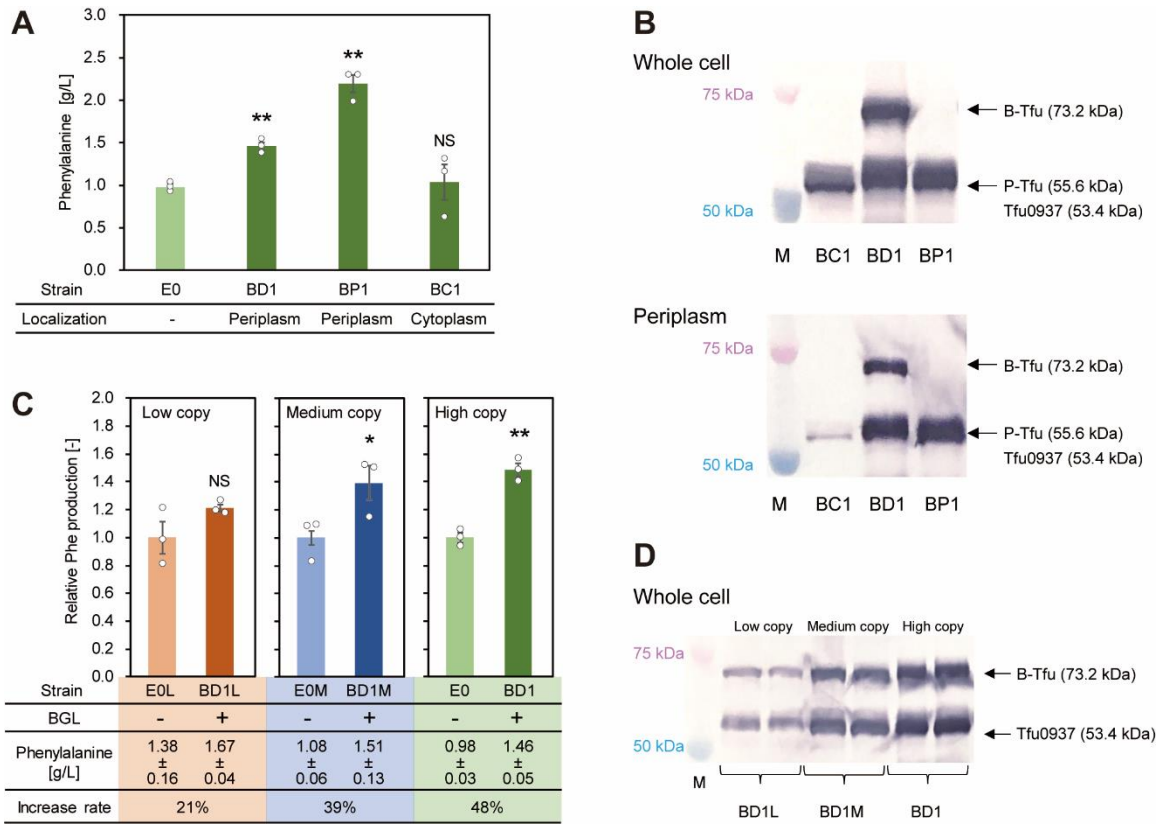

Fig. 1. BGL expression in the *E. coli* periplasm increases Phe production. (A) Phe production after 48 h cultivation in E0, BD1, BP1, and BC1. (B) Immunoblotting of BC1, BD1, and BP1. Leftmost lanes: protein marker. (C) Phe production after 48 h cultivation in E0L, BD1L, E0M, BD1M, E0, and BD1. (D) Immunoblotting of BD1L, BD1M and BD1 (whole-cell extracts). Leftmost lane: protein marker. Data are presented as the average of three independent experiments, and error bars indicate standard error. *P* values were determined using two-tailed Student's t-tests (NS, $P > 0.05$; *$P < 0.05$; **$P < 0.01$). NS: non-significant.

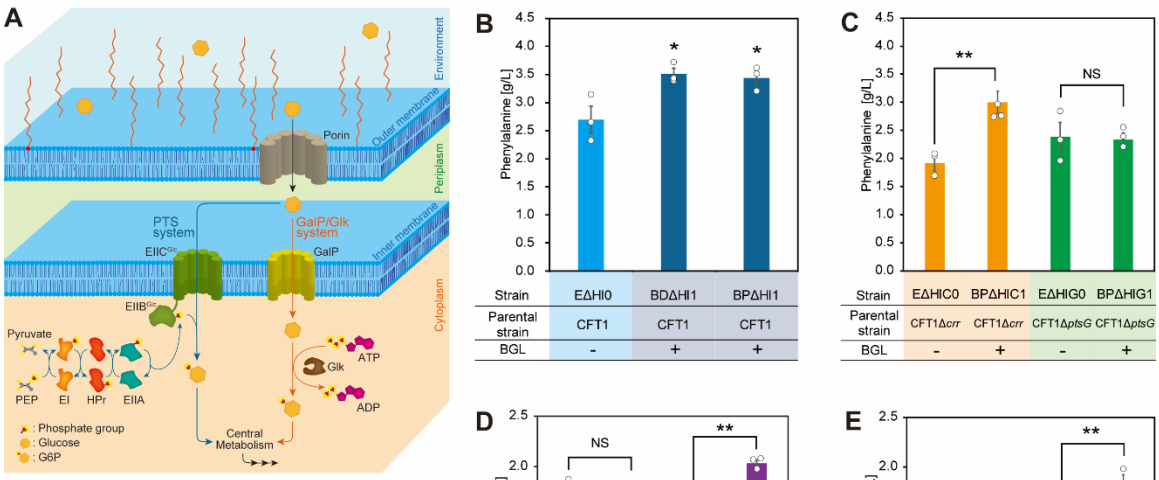

Genes	ptsI	ptsH	crr	ptsG		galP	Glk
Proteins	EI	HPr	EIIA	EIIB	EIIC	GalP	glk
ATCC31882							
CFT1	Δ	Δ				+	+
CFT1Δ*crr*	Δ	Δ	Δ			+	+
CFT1Δ*ptsG*	Δ	Δ		Δ	Δ	+	+
ATCC31882Δ*ptsG*				Δ	Δ		
C421S				X			
dGB				+	Δ		
dGC				Δ	+		

Fig. 2. Periplasmic BGL localization does not affect Phe production in EIIC^{Glc} domain-deficient strains. (A) Glucose transport by the PTS and GalP/Glk system. The lower table indicates disrupted, edited, and overexpressed genes in each strain. "Δ," "X" and "+" indicate gene disruption, inactivating mutation and overexpression, respectively. (B) Phe production after 48 h cultivation. Light- and dark-blue bars indicate the production titers in EΔHI0 (control strain) and BGL-expressing strains (BDΔHI1 and BPΔHI1), respectively. (C) Phe production after 48 h cultivation in EΔHIC0, BPΔHIC1, EΔHIG0 and BPΔHIG1. (D) Phe production after 48 h cultivation in EΔG0, BPΔG1, EC^{421}S0 and BPC^{421}S1. (E) Phe production after 48 h cultivation in EdGB0, BPdGB1, EdGC0, and BPdGC1. Data are presented as the average of three independent experiments, and error bars indicate standard error. *P* values were determined using two-tailed Student's t-tests (NS, $P > 0.05$; *$P < 0.05$; **$P < 0.01$). NS: non-significant.

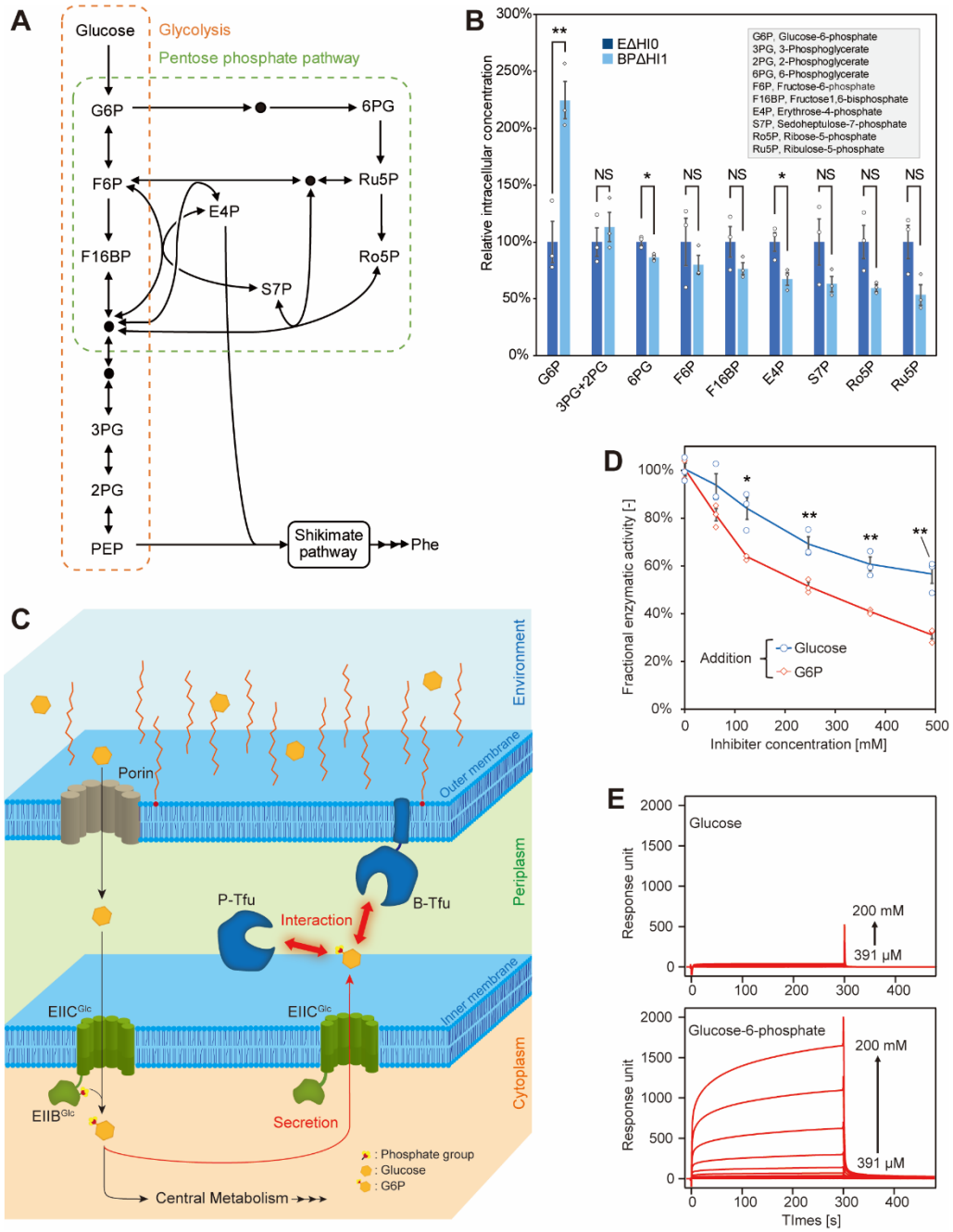

800 **Fig. 3. G6P—a key metabolite, as demonstrated via metabolome analysis.** (A)

801 Metabolism of glucose. (B) Intracellular concentrations of glycolysis and PPP

802 metabolites in BPΔHI1 compared to EΔHI0 (control strain). (C) Diagram of the

803 hypothesized mechanism described in the text. (D) *In vitro* examination of BGL activity

804 inhibition by glucose and G6P. Blue circle and red diamond symbols indicate fractional

805 enzymatic activity with the addition of glucose and G6P, respectively. (E) SPR
806 sensorgrams for β-glucosidase against glucose and G6P. For SPR measurements, the flow
807 rate was 30 μL min^{-1}, the immobilized amount of β-glucosidase was 8000 RU and the
808 analyte concentrations (glucose or G6P) were 391–200 mM. Data are presented as the
809 average of three independent experiments, and error bars indicate standard error. *P* values
810 were determined using two-tailed Student's t-tests (NS, $P > 0.05$; *$P < 0.05$; **$P < 0.01$).
811 NS: non-significant.

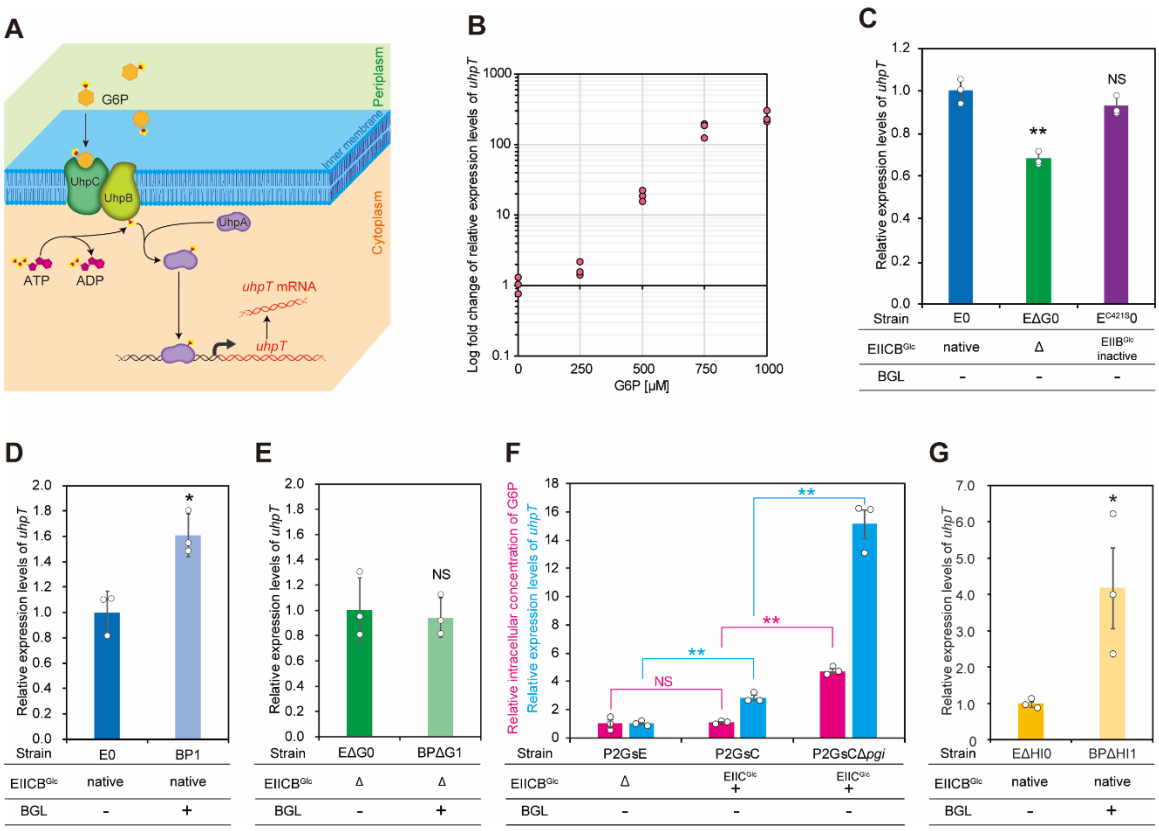

Fig. 4. G6P secretion and accumulation in the periplasm. (A) Diagram of the Uhp system. (B) Relative expression levels of *uhpT* in ATCC 31882 incubated in G6P-supplemented medium. ATCC 31882 was precultured overnight, then washed with LB medium. Subsequently, ATCC31882 was inoculated into LB medium supplemented with each G6P concentration at the initial OD_{600} = 1.0, shaken at 37°C and 1000 rpm for 1 h with Maximizer MBR-022UP (TAITEC, Saitama, Japan), then sampled. (C) Relative *uhpT* expression levels in E0, EΔG0 and $E^{C421S}0$ cultured in a glucose-containing medium. (D) Relative *uhpT* expression levels in E0 and BP1 cultured in a glucose-containing medium. (E) Relative *uhpT* expression levels in EΔG0 and BPΔG1 cultured in a glucose-containing medium. "Δ" indicates gene disruption. "+" indicates overexpression. (F) Relative intracellular G6P concentration (magenta bars) and relative

824 *uhpT* expression levels (cyan bars) in P2GsE, P2GsC and P2GsCΔ*pgi* cultured in a
825 glucose-containing medium. (G) Relative *uhpT* expression levels in EΔHI0 and BPΔHI1
826 cultured in a glucose-containing medium. Data are presented as the mean of three
827 independent experiments, and the error bars indicate the standard error. *P* values were
828 determined using two-tailed Student's t-tests (NS, $P > 0.05$; *$P < 0.05$; **$P < 0.01$). NS:
829 non-significant.

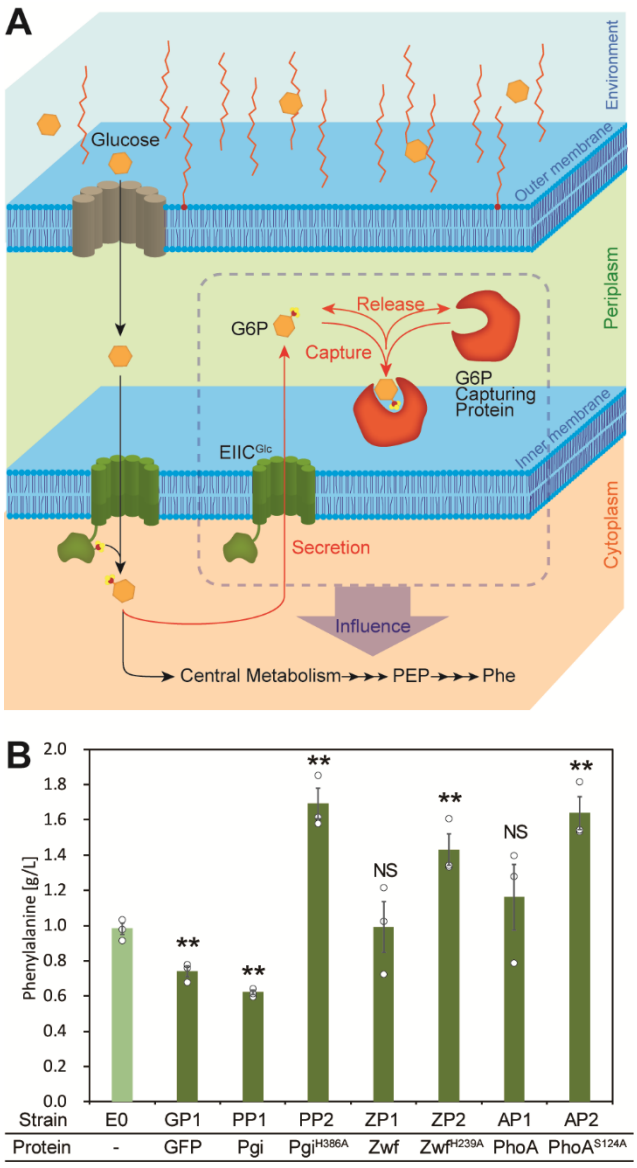

Fig. 5. Application of other proteins using the proposed mechanism. (A) Hypothesized mechanism of G6P transport from the cytoplasm to the periplasm by the EIIC^{Glc} domain and G6P sequestration by the G6P-capturing protein (GCP). (B) Phe production in the periplasmic enzyme-expressing strains after 48 h cultivation. Data are presented as the average of three independent experiments, and the error bars indicate the standard error. *P* values were determined using two-tailed Student's t-tests (NS, $P > 0.05$; *$P < 0.05$; **$P < 0.01$). NS: non-significant.

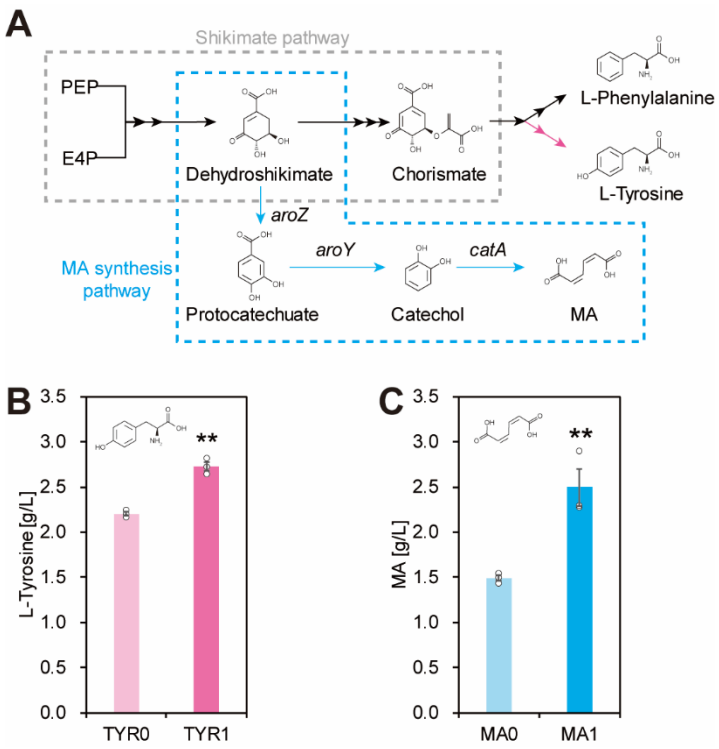

Fig. 6. Production of other metabolites using G6P-capturing proteins. (A) Diagram of the metabolic pathways that synthesize Tyr and MA. (B) Tyr production after 48 h of cultivation in TYR0 and TYR1. (C) MA production after 48 h of cultivation in MA0 and MA1. Data are presented as the average of three independent experiments, and the error bars indicate the standard error. *P* values were determined using two-tailed Student's t-tests (**$P < 0.01$).

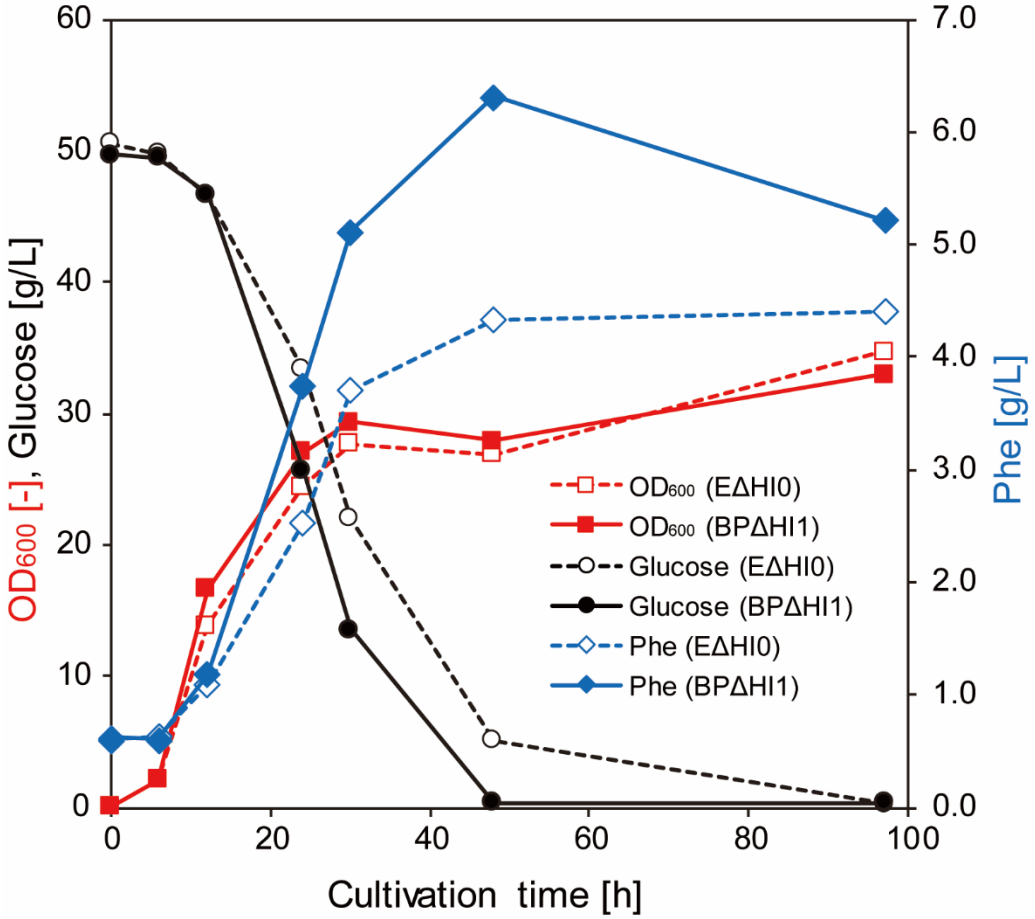

843 **Fig. 7. EΔHI0 and BPΔHI1 culture profiles in a jar fermenter.** Red, black, and blue
844 symbols indicate cell growth, glucose concentration, and Phe concentration, respectively.
845 The EΔHI0 and BPΔHI1 profiles are indicated with dash lines, open symbols, and solid
846 lines, closed symbols, respectively.

847

848

References

Bodelón, G., Palomino, C., Fernández, L.Á., 2013. Immunoglobulin domains in *Escherichia coli* and other enterobacteria: from pathogenesis to applications in antibody technologies. FEMS Microbiol. Rev. 37, 204–250. https://doi.org/10.1111/j.1574-6976.2012.00347.x

Cabell, L.A., Monahan, M.K., Anslyn, E. V., 1999. A competition assay for determining glucose-6-phosphate concentration with a *tris*-boronic acid receptor. Tetrahedron Lett. 40, 7753–7756. https://doi.org/10.1016/S0040-4039(99)01651-2

Chir, J.L., Wan, C.F., Chou, C.H., Wu, A.T., 2011. Hydrolysis of cellulose in synergistic mixtures of β-glucosidase and endo/exocellulase Cel9A from *Thermobifida fusca*. Biotechnol. Lett. 33, 777–782. https://doi.org/10.1007/s10529-010-0500-9

Choi, J.H., Lee, S.Y., 2004. Secretory and extracellular production of recombinant proteins using Escherichia coli. Appl. Microbiol. Biotechnol. 64, 625–635. https://doi.org/10.1007/s00253-004-1559-9

Chung, H., Yang, J.E., Ha, J.Y., Chae, T.U., Shin, J.H., Gustavsson, M., Lee, S.Y., 2015. Bio-based production of monomers and polymers by metabolically engineered microorganisms. Curr. Opin. Biotechnol. 36, 73–84. https://doi.org/10.1016/j.copbio.2015.07.003

Chung Nan Chang, Wun-Jing, K., Chen, E.Y., 1986. Nucleotide sequence of the alkaline phosphatase gene of *Escherichia coli*. Gene 44, 121–125. https://doi.org/10.1016/0378-1119(86)90050-8

Fernández, L.A., 2004. Prokaryotic expression of antibodies and affibodies. Curr. Opin. Biotechnol. 15, 364–373. https://doi.org/10.1016/J.COPBIO.2004.06.004

872 Fujiwara, R., Noda, S., Tanaka, T., Kondo, A., 2020. Metabolic engineering of
873 *Escherichia coli* for shikimate pathway derivative production from glucose–xylose
874 co-substrate. Nat. Commun. 11, 1–12. https://doi.org/10.1038/s41467-019-14024-1
875 Fujiwara, R., Noda, S., Tanaka, T., Kondo, A., 2018. Muconic acid production using
876 gene-level fusion proteins in *Escherichia coli*. ACS Synth. Biol. 7, 2698–2705.
877 https://doi.org/10.1021/acssynbio.8b00380
878 Georgiou, G., Segatori, L., 2005. Preparative expression of secreted proteins in bacteria:
879 status report and future prospects. Curr. Opin. Biotechnol. 16, 538–545.
880 https://doi.org/10.1016/j.copbio.2005.07.008
881 Gonzalez-Perez, D., Ratcliffe, J., Tan, S.K., Wong, M.C.M., Yee, Y.P., Nyabadza, N.,
882 Xu, J.-H., Wong, T.S., Tee, K.L., 2021. Random and combinatorial mutagenesis for
883 improved total production of secretory target protein in Escherichia coli. Sci. Rep.
884 11, 5290. https://doi.org/10.1038/s41598-021-84859-6
885 Heng, S.S.J., Chan, O.Y.W., Keng, B.M.H., Ling, M.H.T., 2011. Glucan biosynthesis
886 protein G is a suitable reference gene in *Escherichia coli* K-12. ISRN Microbiol.
887 2011, 469053. https://doi.org/10.5402/2011/469053
888 Hernández-Montalvo, V., Martínez, A., Hernández-Chavez, G., Bolivar, F., Valle, F.,
889 Gosset, G., 2003. Expression of *galP* and *glk* in a *Escherichia coli* PTS mutant
890 restores glucose transport and increases glycolytic flux to fermentation products.
891 Biotechnol. Bioeng. 83, 687–694. https://doi.org/10.1002/bit.10702
892 Ikeda, N., Miyamoto, M., Adachi, N., Nakano, M., Tanaka, T., Kondo, A., 2013. Direct
893 cadaverine production from cellobiose using β-glucosidase displaying *Escherichia*
894 *coli*. AMB Express 3, 1–7. https://doi.org/10.1186/2191-0855-3-67

Jacob-Dubuisson, F., Mechaly, A., Betton, J.-M., Antoine, R., 2018. Structural insights into the signalling mechanisms of two-component systems. Nat. Rev. Microbiol. 2018 1610 16, 585–593. https://doi.org/10.1038/s41579-018-0055-7

Jiang, Y., Chen, B., Duan, C., Sun, B., Yang, J., Yang, S., 2015. Multigene editing in the *Escherichia coli* genome via the CRISPR-Cas9 system. Appl. Environ. Microbiol. 81, 2506–2514. https://doi.org/10.1128/AEM.04023-14

Juminaga, D., Baidoo, E.E.K., Redding-Johanson, A.M., Batth, T.S., Burd, H., Mukhopadhyay, A., Petzold, C.J., Keasling, J.D., 2012. Modular engineering of L-tyrosine production in *Escherichia coli*. Appl. Environ. Microbiol. 78, 89–98. https://doi.org/10.1128/AEM.06017-11

Kurumbang, N.P., Vera, J.M., Hebert, A.S., Coon, J.J., Landick, R., 2020. Heterologous expression of a glycosyl hydrolase and cellular reprogramming enable *Zymomonas mobilis* growth on cellobiose. PLoS One 15, e0226235. https://doi.org/10.1371/journal.pone.0226235

Lian, J., McKenna, R., Rover, M.R., Nielsen, D.R., Wen, Z., Jarboe, L.R., 2016. Production of biorenewable styrene: utilization of biomass-derived sugars and insights into toxicity. J. Ind. Microbiol. Biotechnol. 43, 595–604. https://doi.org/10.1007/s10295-016-1734-x

Long, C.P., Au, J., Sandoval, N.R., Gebreselassie, N.A., Antoniewicz, M.R., 2017. Enzyme I facilitates reverse flux from pyruvate to phosphoenolpyruvate in Escherichia coli. Nat. Commun. 8, 14316. https://doi.org/10.1038/ncomms14316

Lütke-Eversloh, T., Stephanopoulos, G., 2007. L-Tyrosine production by deregulated strains of *Escherichia coli*. Appl. Microbiol. Biotechnol. 75, 103–110. https://doi.org/10.1007/s00253-006-0792-9

Malherbe, G., Humphreys, D.P., Davé, E., 2019. A robust fractionation method for protein subcellular localization studies in *Escherichia coli*. Biotechniques 66, 171–178. https://doi.org/10.2144/btn-2018-0135

Mirzadeh, K., Shilling, P.J., Elfageih, R., Cumming, A.J., Cui, H.L., Rennig, M., Nørholm, M.H.H., Daley, D.O., 2020. Increased production of periplasmic proteins in *Escherichia coli* by directed evolution of the translation initiation region. Microb. Cell Fact. 19, 85. https://doi.org/10.1186/s12934-020-01339-8

Morrison, J.F., 1969. Kinetics of the reversible inhibition of enzyme-catalysed reactions by tight-binding inhibitors. Biochim. Biophys. Acta - Enzymol. 185, 269–286. https://doi.org/10.1016/0005-2744(69)90420-3

Nakagawa, A., Minami, H., Kim, J.-S., Koyanagi, T., Katayama, T., Sato, F., Kumagai, H., 2011. A bacterial platform for fermentative production of plant alkaloids. Nat. Commun. 2, 326. https://doi.org/10.1038/ncomms1327

Nielsen, J., Keasling, J.D., 2016. Engineering Cellular Metabolism. Cell 164, 1185–1197. https://doi.org/10.1016/J.CELL.2016.02.004

Niu, H., Li, R., Liang, Q., Qi, Q., Li, Q., Gu, P., 2019. Metabolic engineering for improving L- tryptophan production in *Escherichia coli*. J. Ind. Microbiol. Biotechnol. 46, 55–65. https://doi.org/10.1007/s10295-018-2106-5

Noda, S., Kondo, A., 2017. Recent advances in microbial production of aromatic chemicals and derivatives. Trends Biotechnol. 35, 785–796. https://doi.org/10.1016/j.tibtech.2017.05.006

Noda, S., Shirai, T., Oyama, S., Kondo, A., 2016. Metabolic design of a platform *Escherichia coli* strain producing various chorismate derivatives. Metab. Eng. 33, 119–129. https://doi.org/10.1016/j.ymben.2015.11.007

Nonaka, D., Fujiwara, R., Hirata, Y., Tanaka, T., Kondo, A., 2021. Metabolic engineering of 1,2-propanediol production from cellobiose using beta-glucosidase-expressing E. coli. Bioresour. Technol. 329, 124858. https://doi.org/10.1016/j.biortech.2021.124858

Olson, M.M., Templeton, L.J., Suh, W., Youderian, P., Sariaslani, F.S., Gatenby, A.A., Van Dyk, T.K., 2007. Production of tyrosine from sucrose or glucose achieved by rapid genetic changes to phenylalanine-producing *Escherichia coli* strains. Appl. Microbiol. Biotechnol. 74, 1031–1040. https://doi.org/10.1007/s00253-006-0746-2

Poddar, A., Azam, M.S., Kayikcioglu, T., Bobrovskyy, M., Zhang, J., Ma, X., Labhsetwar, P., Fei, J., Singh, D., Luthey-Schulten, Z., Vanderpool, C.K., Ha, T., 2021. Effects of individual base-pairs on in vivo target search and destruction kinetics of bacterial small RNA. Nat. Commun. 12, 1–15. https://doi.org/10.1038/s41467-021-21144-0

Rodriguez, A., Martínez, J. a, Báez-Viveros, J.L., Flores, N., Hernández-Chávez, G., Ramírez, O.T., Gosset, G., Bolivar, F., 2013. Constitutive expression of selected genes from the pentose phosphate and aromatic pathways increases the shikimic

959 acid yield in high-glucose batch cultures of an *Escherichia coli* strain lacking PTS
960 and *pykF*. Microb. Cell Fact. 12, 86. https://doi.org/10.1186/1475-2859-12-86
961 Satowa, D., Fujiwara, R., Uchio, S., Nakano, M., Otomo, C., Hirata, Y., Matsumoto, T.,
962 Noda, S., Tanaka, T., Kondo, A., 2020. Metabolic engineering of *E. coli* for
963 improving mevalonate production to promote NADPH regeneration and enhance
964 acetyl- CoA supply. Biotechnol. Bioeng. 117, 2153–2164.
965 https://doi.org/10.1002/bit.27350
966 Schmidt T., 2019. Encyclopedia of Microbiology, 4th Editio. ed. Academic Press,
967 Amsterdam.
968 Shen, X., Wang, Jia, Wang, Jian, Chen, Z., Yuan, Q., Yan, Y., 2017. High-level De novo
969 biosynthesis of arbutin in engineered *Escherichia coli*. Metab. Eng. 42, 52–58.
970 https://doi.org/10.1016/j.ymben.2017.06.001
971 Shirai, T., Matsuda, F., Okamoto, M., Kondo, A., 2013. Evaluation of control
972 mechanisms for *Saccharomyces cerevisiae* central metabolic reactions using
973 metabolome data of eight single-gene deletion mutants. Appl. Microbiol.
974 Biotechnol. 97, 3569–3577. https://doi.org/10.1007/s00253-012-4597-8
975 Sochacki, K.A., Shkel, I.A., Record, M.T., Weisshaar, J.C., 2011. Protein diffusion in the
976 periplasm of *E. coli* under osmotic stress. Biophys. J. 100, 22–31.
977 https://doi.org/10.1016/j.bpj.2010.11.044
978 Soma, Y., Inokuma, K., Tanaka, T., Ogino, C., Kondo, A., Okamoto, M., Hanai, T.,
979 2012. Direct isopropanol production from cellobiose by engineered *Escherichia coli*
980 using a synthetic pathway and a cell surface display system. J. Biosci. Bioeng. 114,
981 80–85. https://doi.org/10.1016/j.jbiosc.2012.02.019

Spiridonov, N.A., Wilson, D.B., 2001. Cloning and biochemical characterization of BglC, a β-glucosidase from the cellulolytic actinomycete *Thermobifida fusca*. Curr. Microbiol. 42, 295–301. https://doi.org/10.1007/s002840110220

Stock, J.B., Rauch, B., Roseman, S., 1977. Periplasmic space in *Salmonella typhimurium* and *Escherichia coli*. J. Biol. Chem. 252, 7850–7861. https://doi.org/10.1016/S0021-9258(17)41044-1

Sun, J., Lin, Y., Shen, X., Jain, R., Sun, X., Yuan, Q., Yan, Y., 2016. Aerobic biosynthesis of hydrocinnamic acids in *Escherichia coli* with a strictly oxygen-sensitive enoate reductase. Metab. Eng. 35, 75–82. https://doi.org/10.1016/j.ymben.2016.02.002

Tanaka, T., Kawabata, H., Ogino, C., Kondo, A., 2011. Creation of a cellooligosaccharide-assimilating *Escherichia coli* strain by displaying active beta-glucosidase on the cell surface via a novel anchor protein. Appl. Environ. Microbiol. 77, 6265–70. https://doi.org/10.1128/AEM.00459-11

Thompson, B., Pugh, S., Machas, M., Nielsen, D.R., 2018. Muconic acid production via alternative pathways and a synthetic "Metabolic Funnel." ACS Synth. Biol. 7, 565–575. https://doi.org/10.1021/acssynbio.7b00331

Västermark, A., Saier, M.H., 2014. The involvement of transport proteins in transcriptional and metabolic regulation. Curr. Opin. Microbiol. 18, 8–15. https://doi.org/10.1016/j.mib.2014.01.002

Verhamme, D.T., Arents, J.C., Postma, P.W., Crielaard, W., Hellingwerf, K.J., 2001. Glucose-6-phosphate-dependent phosphoryl flow through the Uhp two-component

regulatory system. Microbiology 147, 3345–3352. https://doi.org/10.1099/00221287-147-12-3345

Verhamme, D.T., Postma, P.W., Crielaard, W., Hellingwerf, K.J., 2002. Cooperativity in signal transfer through the Uhp system of *Escherichia coli*. J. Bacteriol. 184, 4205–4210. https://doi.org/10.1128/JB.184.15.4205-4210.2002

Wu, W., Guo, X., Zhang, M., Huang, Q., Qi, F., Huang, J., 2018. Enhancement of L-phenylalanine production in *Escherichia coli* by heterologous expression of Vitreoscilla hemoglobin. Biotechnol. Appl. Biochem. 65, 476–483. https://doi.org/10.1002/bab.1605

Zhang, H., Pereira, B., Li, Z., Stephanopoulos, G., 2015. Engineering *Escherichia coli* coculture systems for the production of biochemical products. Proc. Natl. Acad. Sci. 112, 8266–8271. https://doi.org/10.1073/pnas.1506781112

Zheng, H., Taraska, J., Merz, A.J., Gonen, T., 2010. The prototypical H+/galactose symporter GalP assembles into functional trimers. J. Mol. Biol. 396, 593–601. https://doi.org/10.1016/j.jmb.2009.12.010

Zhou, H., Liao, X., Wang, T., Du, G., Chen, J., 2010. Enhanced l-phenylalanine biosynthesis by co-expression of *pheA*^{fbr} and *aroF*^{wt}. Bioresour. Technol. 101, 4151–4156. https://doi.org/10.1016/j.biortech.2010.01.043

Supplementary materials

This file includes:

Figures S1 to S5

Supplementary discussion 1

Tables S1 to S3

SI References

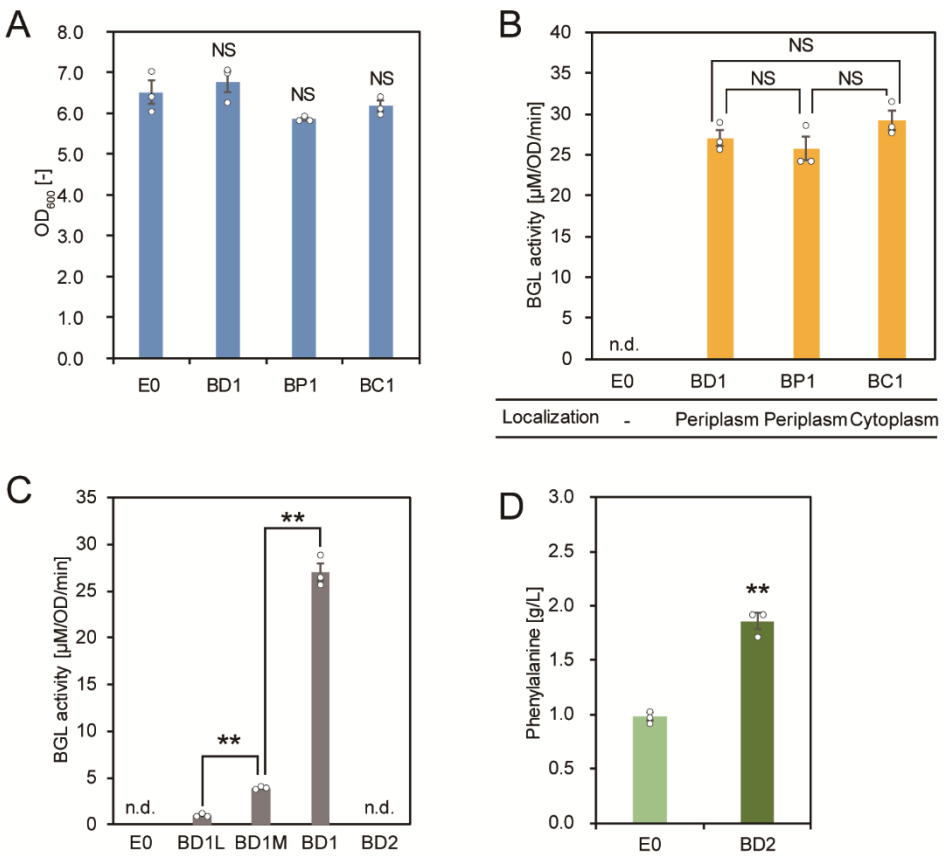

Fig. S1. Effect of BGL expression level or enzymatic activity on Phe production. (A) Bacterial cell growth in glucose medium. Blue bars indicate the OD600 of the control strain (E0) and strains expressing Blc-Tfu0937, PelB-Tfu0937, and Tfu0937 (BD1, BP1, and BC1, respectively). (B) Whole-cell activity of BGL in E0, BD1, BP1 and BC1. (C) Whole-cell activity of BGL in E0, BD1L, BD1M, BD1 and BD2. (D) L-phenylalanine production after 48 h cultivation in E0 and a strain expressing inactivated BGL (BD2). n.d., not detected. Data are presented as the average of three independent experiments, and error bars indicate standard error. *P* values were determined using two-tailed Student's t-tests (NS, $P > 0.05$; $^{**}P < 0.01$). BGL, β-glucosidase; NS, non-significant.

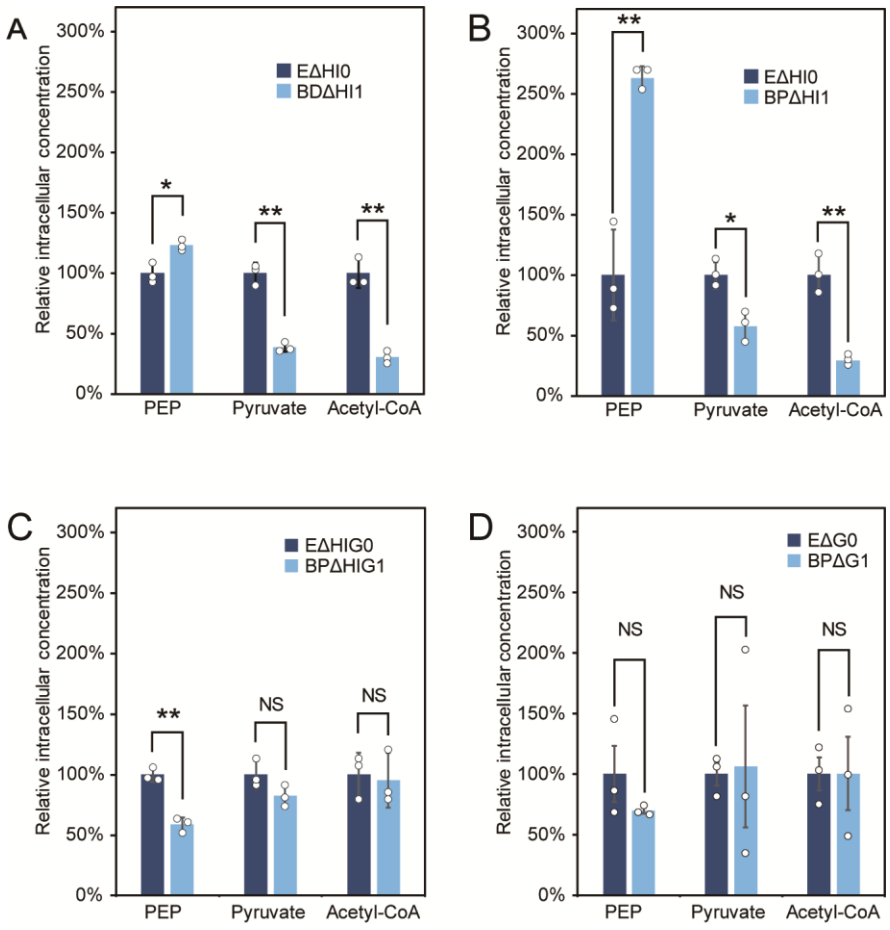

Fig. S2. Intracellular PEP, pyruvate, and acetyl-CoA concentrations. Intracellular PEP, pyruvate, and acetyl-CoA concentrations in BDΔHI1 relative to EΔHI0 (A), BPΔHI1 relative to EΔHI0 (B), BPΔHIG1 relative to EΔHIG0 (C) and BPΔG1 relative to EΔG0 (D). Data are presented as the mean of three independent experiments, and error bars indicate standard error. *P* values were determined using two-tailed Student's t-tests (NS, $P > 0.05$; *$P < 0.05$; **$P < 0.01$). NS, non-significant; PEP, phosphoenolpyruvate.

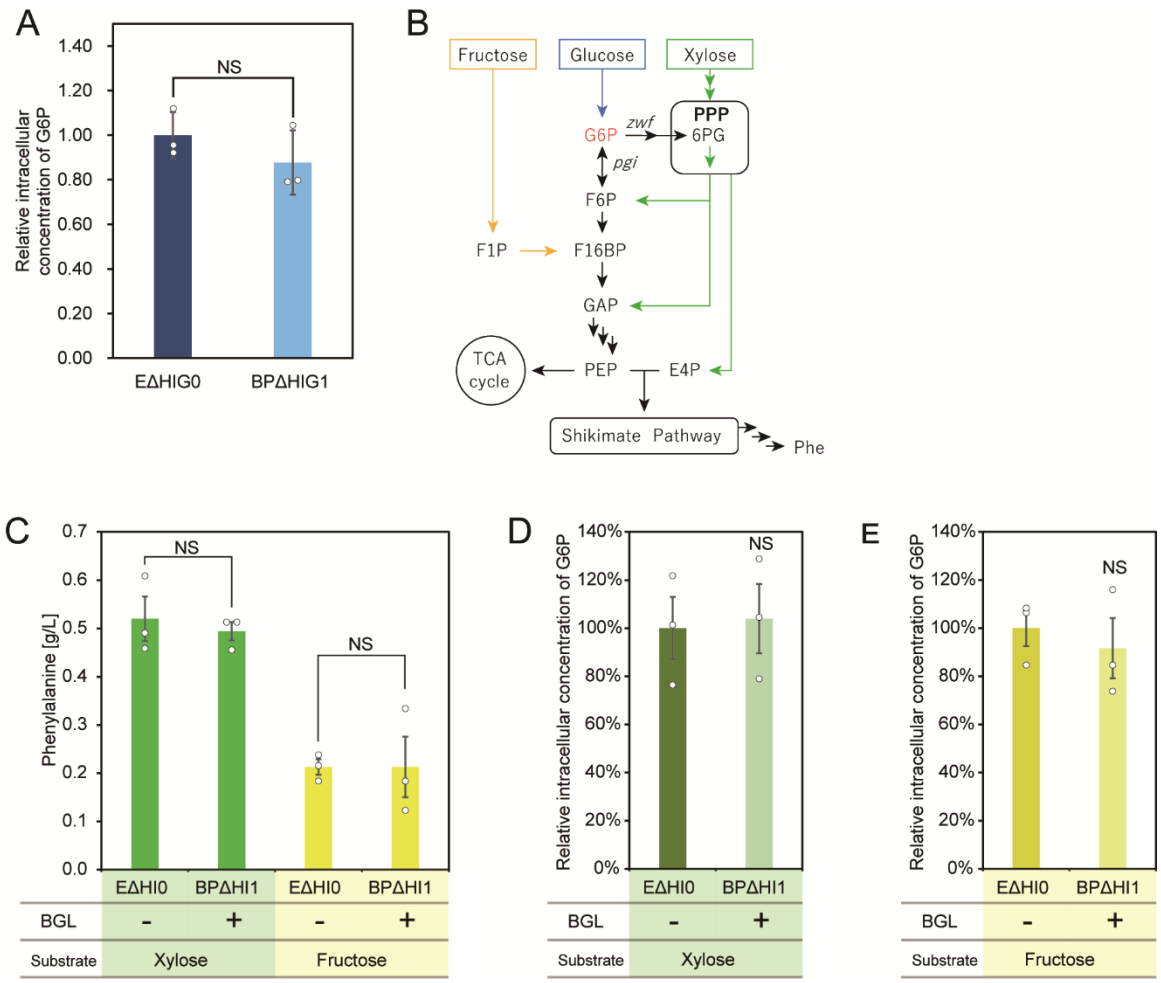

Fig. S3. Metabolome analysis of glycolysis and the PPP in strains with periplasmic BGL localization. (A) Intracellular G6P concentrations in BPΔHIG1 relative to EΔHIG0 (control strain). (B) Catabolic pathway for glucose, xylose and fructose. (C) Phe production after 48 h cultivation in BPΔHI1 and EΔHI0 using xylose or fructose as a carbon source. (D) Intracellular G6P concentrations with xylose as the substrate in BPΔHI1 relative to EΔHI0. (E) Intracellular G6P concentrations with fructose as the substrate in BPΔHI1 relative to EΔHI0. Data are presented as the mean of three independent experiments, and error bars indicate standard errors. *P* values were determined using two-tailed Student's t-tests (NS, $P > 0.05$; *$P < 0.05$; **$P < 0.01$). BGL, β-glucosidase; G6P, glucose-6-phosphate; NS, non-significant; PPP, pentose phosphate pathway.

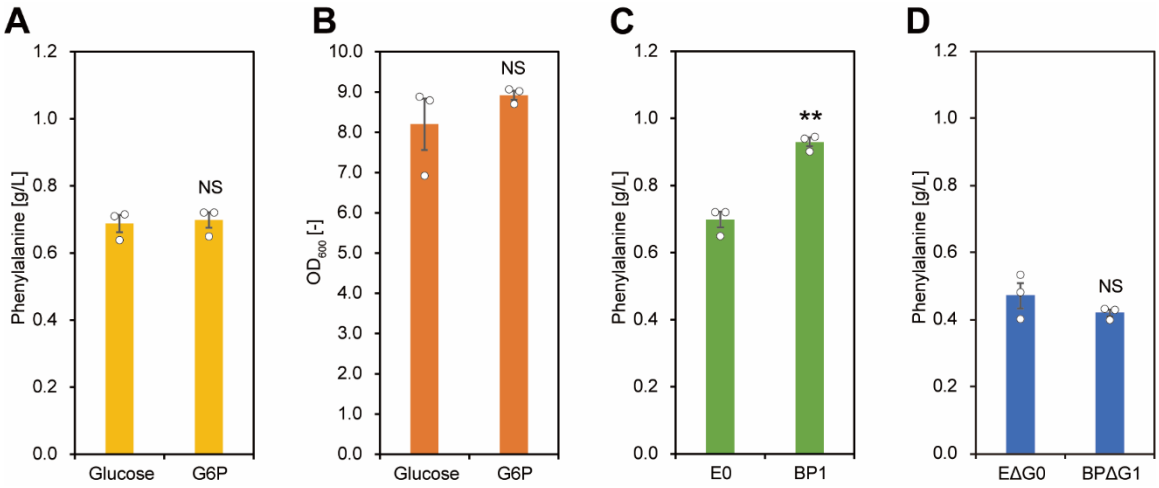

Fig. S4. Phe production in G6P-containing medium. Analysis of *uhpT* expression. (A) Phe production in strain E0 cultured in media containing 55.5 mM glucose or G6P. (B) Bacterial cell growth of E0 cultured in media containing 55.5 mM glucose or G6P. (C) L-phenylalanine production in E0 and BP1 cultured in media containing 55.5 mM G6P. (D) L-phenylalanine production in EΔG0 and BPΔG1 cultured in media containing 55.5 mM G6P. Data are presented as the mean of three independent experiments, and error bars indicate standard error. *P* values were computed using two-tailed Student's *t*-test (NS, $P > 0.05$; **, $P < 0.01$). G6P, glucose-6-phosphate.

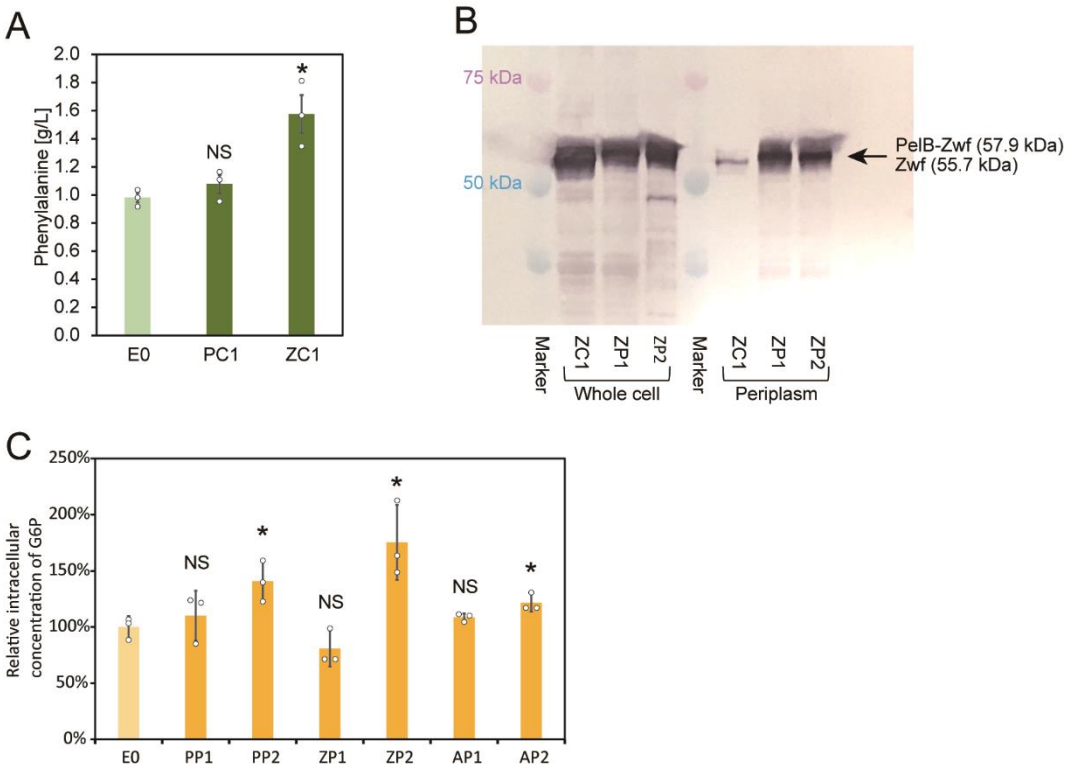

Fig. S5. Analysis of the application of G6P-capturing proteins. (A) L-phenylalanine production after 48 h cultivation in Pgi and Zwf overexpression strains. Light- and dark-green bars indicate L-phenylalanine production by E0 (control strain) and strains expressing native Pgi and Zwf in the cytoplasm (PC1 and ZC1), respectively. (B) Western blotting of Zwf. As indicated in the figure, the left four lanes correspond to a molecular weight protein marker and whole-cell extract samples (ZC1, ZP1, and ZP2). The right four lanes correspond to a protein marker and periplasmic extract samples (ZC1, ZP1, and ZP2). Zwf expression levels in the periplasmic extracts of strains ZP1 and ZP2 were 6.1- and 5.8-times higher than those in ZC1. An ANTI-FLAG M2 monoclonal antibody (Sigma-Aldrich) and an anti-rabbit IgG (Fc) AP conjugate (Promega Corp.) were used to detect Zwf and PelB-Zwf fused with a FLAG-tag. (C) Intracellular G6P concentrations in strains expressing G6P-capturing proteins in the periplasm relative to E0 (control strain). Data are presented as the mean of three

independent experiments, and error bars indicate standard error. *P* values were computed using two-tailed Student's t-test (NS, $P > 0.05$; $*P < 0.05$). G6P, glucose-6-phosphate.

Supplementary discussion 1

The assumed reaction mechanism, in which one GCP molecule captures one G6P molecule to form a GCP-G6P complex, then dissociating to GCP and G6P, is shown in Eq. 2:

$$GCP + G6P \leftrightharpoons GCP\text{-}G6P \quad \text{(Eq. 2)}$$

Assuming that this reaction has reached the equilibrium rapidly, the dissociation constant (K_d) is set as follows.

$$K_d = \frac{[GCP][G6P]}{[GCP\text{-}G6P]} \quad \text{(Eq. 3)}$$

Focusing on the periplasmic concentration of the GCP-G6P complex, converting Eq. 3 results in the following Eq. 4.

$$[GCP\text{-}G6P]_P = \frac{[GCP]_P[G6P]_P}{K_d} \quad \text{(Eq. 4)}$$

$[GCP\text{-}G6P]_P$, $[GCP]_P$, and $[G6P]_P$ indicate the periplasmic concentration of the GCP-G6P complex, free GCP, and freeG6P, respectively. The total concentration of the periplasmic GCP ($[GCP]_{P0}$) is the sum of $[GCP]_P$ and $[GCP\text{-}G6P]_P$, Eq. 4 results in the following Eq. 5.

$$[GCP\text{-}G6P]_P = \frac{[G6P]_P[GCP]_{P0}}{[G6P]_P + K_d} \quad \text{(Eq. 5)}$$

The total concentration of the periplasmic G6P ($[G6P]_{P0}$) is the sum of $[G6P]_P$ and $[GCP\text{-}G6P]_P$, Eq. 5 results in the following Eq. 6.

$$[G6P]_{P0} = \left(1 + \frac{[GCP]_{P0}}{[G6P]_P + K_d}\right) \cdot [G6P]_P \quad \text{(Eq. 6)}$$

Eq.6 means that even if the periplasmic concentration of free G6P is the same, the total G6P concentration in the periplasm (including free G6P and GCP-G6P complex) is higher when GCP is present in the periplasm.

Table S1. Strains and plasmids used in this study

Strains	Genotype	Source or reference
ATCC31882	L-Phenylalanine-overproducing strain	ATCC
ATCC31882Δ*ptsG*	ATCC31882Δ*ptsG*	This study
CFT1	ATCC31882 *ptsHI::P* $_{A1lacO-1}$ *-glk-galP*	Noda et al., 2016
CFT1Δ*crr*	ATCC31882 *ptsHI::P* $_{A1lacO-1}$ *-glk-galP* Δ*crr*	This study
CFT1Δ*ptsG*	ATCC31882 *ptsHI::P* $_{A1lacO-1}$ *-glk-galP* Δ*ptsG*	This study
CFT1Δ*pheA*	ATCC31882 *ptsHI::P* $_{A1lacO-1}$ *-glk-galP* Δ*pheA*	This study
C421S	ATCC31882 *ptsG::ptsG*^{C421S}	This study
P2Gs	ATCC31882 *ptsG::P* $_{A1lacO-1}$ *-glk-galP* Δ*sgrS*	This study
P2GsΔ*pgi*	ATCC31882 *ptsG::P* $_{A1lacO-1}$ *-glk-galP* Δ*sgrS* Δ*pgi*	This study
TYR	ATCC31882 *trpE::tyrA*^{fbr} Δ*pheA*	This study
E0	ATCC31882 harboring pHLA	This study
BD1	ATCC31882 harboring pHLA-blc-Tfu0937	This study
E0L	ATCC31882 harboring pSAK	This study
BD1L	ATCC31882 harboring pSAK-blc-Tfu0937	This study
E0M	ATCC31882 harboring pZA23MCS	This study
BD1M	ATCC31882 harboring pZA23-blc-Tfu0937	This study
BD2	ATCC31882 harboring pHLA-blc-Tfu0937E^{388}A	This study
BP1	ATCC31882 harboring pHLA-pelB-Tfu0937	This study
BC1	ATCC31882 harboring pHLA-Tfu0937	This study
EΔHI0	CFT1 harboring pHLA	This study
BDΔHI1	CFT1 harboring pHLA-blc-Tfu0937	This study
BPΔHI1	CFT1 harboring pHLA-pelB-Tfu0937	This study
EΔHIC0	CFT1Δ*crr* harboring pHLA	This study
BPΔHIC1	CFT1Δ*crr* harboring pHLA-pelB-Tfu0937	This study
EΔHIG0	CFT1Δ*ptsG* harboring pHLA	This study
BPΔHIG1	CFT1Δ*ptsG* harboring pHLA-pelB-Tfu0937	This study
EΔG0	ATCC31882Δ*ptsG* harboring pHLA	This study
BPΔG1	ATCC31882Δ*ptsG* harboring pHLA-pelB-Tfu0937	This study
E^{C421S}0	C421S harboring pHLA	This study
BP^{C421S}1	C421S harboring pHLA-prlB-Tfu0937	This study

dGB	ATCC31882Δ*ptsG* harboring pZA23-EIIB^{Glc}	This study
dGC	ATCC31882Δ*ptsG* harboring pZA23-EIIC^{Glc}	This study
EdGB0	dGB harboring pHLA	This study
BPdGB1	dGB harboring pHLA pHLA-pelB-Tfu0937	This study
EdGC0	dGC harboring pHLA	This study
BPdGC1	dGC harboring pHLA pHLA-pelB-Tfu0937	This study
P2GsE	P2Gs harboring pZA23-MCS	This study
P2GsC	P2Gs harboring pZA23-EIIC^{Glc}	This study
P2GsCΔ*pgi*	P2GsΔ*pgi* harboring pZA23-EIIC^{Glc}	This study
AP1	ATCC31882 harboring pHLA-pelB-phoA	This study
AP2	ATCC31882 harboring pHLA-pelB-phoAS^{124}A	This study
PP1	ATCC31882 harboring pHLA-pelB-pgi	This study
PP2	ATCC31882 harboring pHLA-pelB-pgiH^{386}A	This study
PC1	ATCC31882 harboring pHLA-pgi	This study
ZP1	ATCC31882 harboring pHLA-pelB-zwf	This study
ZP2	ATCC31882 harboring pHLA-pelB-zwfH^{239}A	This study
ZC1	ATCC31882 harboring pHLA-zwf	This study
GP1	ATCC31882 harboring pHLA-pelB-gfp	This study
TYR0	TYR harboring pHLA	This study
TYR1	TYR harboring pHLA-blc-Tfu0937	This study
MA0	CFT1Δ*pheA* harboring pSAK-ZYc and pHLA	This study
MA1	CFT1Δ*pheA* harboring pSAK-ZYc and pHLA-pelB-Tfu0937	This study
Plasmids		
pHLA	P_{HCE}, *ColE1 ori*, *Amp*^{r}	Tanaka et al., 2011
pHLA-blc-Tfu0937	pHLA expressing Blc-Tfu0937	This study
pHLA-blc-Tfu0937^{E388A}	pHLA expressing Blc-Tfu0937E^{388}A	This study
pHLA-pelB-Tfu0937	pHLA expressing PelB-Tfu0937	This study
pHLA-Tfu0937	pHLA expressing Tfu0937	This study
pHLA-blc-Tfu0937-FLAG	pHLA expressing Blc-Tfu0937E^{388}A fused with FLAG-tag	This study
pHLA-pelB-Tfu0937-FLAG	pHLA expressing PelB-Tfu0937 fused with FLAG-tag	This study
pHLA-Tfu0937-FLAG	pHLA expressing Tfu0937 fused with FLAG-tag	This study

pHLA-pelB-phoA	pHLA expressing PelB-PhoA	This study
pHLA-pelB-phoA^{S124A}	pHLA expressing PelB-PhoAS^{124}A	This study
pHLA-pelB-pgi	pHLA expressing PelB-Pgi	This study
pHLA-pelB-pgi^{H386A}	pHLA expressing PelB-PgiH^{386}A	This study
pHLA-pgi	pHLA expressing Pgi	This study
pHLA-pelB-zwf	pHLA expressing PelB-Zwf	This study
pHLA-pelB-zwf^{H239A}	pHLA expressing PelB-ZwfH^{239}A	This study
pHLA-zwf	pHLA expressing Zwf	This study
pHLA-pelB-zwf-FLAG	pHLA expressing PelB-Zwf fused with FLAG-tag	This study
pHLA-pelB-zwf^{H239A}-FLAG	pHLA expressing PelB-ZwfH^{239}A fused with FLAG-tag	This study
pHLA-zwf-FLAG	pHLA expressing Zwf fused with FLAG-tag	This study
pHLA-pelB-gfp	pHLA expressing PelB-GFP	This study
pSAK	P_{AlacO1}, *SC101 ori*, and Cm^r	Noda et al., 2017
pSAK-blc-Tfu0937	pSAK expressing Blc-Tfu0937	This study
pSAK-blc-Tfu0937-FLAG	pSAK expressing Blc-Tfu0937 fused with FLAG-tag	This study
pSAK-P_{trc}	P_{trc}, *SC101 ori*, and Cm^r	Fujiwara et al., 2020
pSAK-ZYc	pSAK-P_{trc} containing *aroZ*, *aroY*, and *catA*	Fujiwara et al., 2020
pSAK-*tyrA*^{fbr}	pSAK-P_{trc} containing *tyrA*^{fbr} and feedback-inhibition-resistant (fbr) derivatives of *tyrA*	Fujiwara et al., 2020
pZA23MCS	$P_{A1lacO-1}$, *p15A ori*, Km^r	Expressys
pZA23-blc-Tfu0937	pZA23MCS expressing Blc-Tfu0937	This study
pZA23-blc-Tfu0937	pZA23MCS expressing Blc-Tfu0937 fused with FLAG-tag	This study
pZA23-EIIB^{Glc}	pHLA expressing EIIB^{Glc} domain	This study
pZA23-EIIC^{Glc}	pHLA expressing EIIC^{Glc} domain	This study
pTargetF	Constitutive expression of sgRNA	Addgene
pCas	Constitutive expression of cas9 and inducible expression of λ RED and sgR	Addgene
pTΔptsG	Constitutive expression of sgRNA with donor-editing template DNA for *ptsG* disruption	This study
pTΔcrr	Constitutive expression of sgRNA with donor-editing template DNA for *crr* disruption	This study
pTΔpheA	Constitutive expression of sgRNA with donor-editing template DNA for *pheA* disruption	Fujiwara et al., 2020

pTΔsgrS	Constitutive expression of sgRNA with donor-editing template DNA for *sgrS* disruption	This study
pTΔpgi	Constitutive expression of sgRNA with donor-editing template DNA for *pgi* disruption	This study
pTtrpE::tyr^{fbr}	Constitutive expression of sgRNA with donor-editing template DNA for *tyrA*^{fbr} insertion in *trpE* locus	This study
pTptsG::galP-glk	Constitutive expression of sgRNA with donor-editing template DNA for *galP-glk* insertion in *ptsG* locus	This study

Table S2. Primers used in the present study

Plasmids	Primers	Sequences
pHLA-blc-tfu0937^{E388A}	E388A_for	CTACCCGGGCCTGCCGCTGTACATCACCGCGAACGGCGCCGCCTTCGAGGAC
	E388A_re	GTCCTCGAAGGCGGCGCCGTTCGCGGTGATGTACAGCGGCAGGCCCGGGTAG
pHLA-pelB-tfu0937	pelB_Tfu0937_f1	CCGCTGCTGCTGGTCTGCTGCTCCTCGCTGCCCAGCCGGCGATGGCCATGACCTCGCAATCGACGACTCC
	XhoI_Tfu0937_re	GCCAAGCTTCTCGAGCTATTCCTGTCCGAAGATTCCCCCG
	Bgl2_pelB_for	TGGAAAAAGGAGATCTGATGAAATACCTGCTGCCGACCGCTGCTGCTGGTCTGCTGC
pHLA-tfu0937	n.s._tfu0937_f	TGGAAAAAGGAGATCTGATGACCTCGCAATCGACGACTCC
	n.s._tfu0937_r	GCCAAGCTTCTCGAGCTATTCCTGTCCGAAGATTCCCCCG
pHLA-phoA	phoA_f	TGGAAAAAGGAGATCTGATGAAACAAAGCACTATTGCACTGGCACTCTTACCG
	phoA_r	AGCCAAGCTTCTCGAGTTATTTCAGCCCCAGAGCGGCTTTC
pHLA-phoA^{S124A}	phoA_S124A_f	GTTGCTGATGCGGCCGCGTCGGTGACGTAGTCCGGTTTGCCG
	phoA_S124A_r	CGTCACCGACGCGGCCGCATCAGCAACCGCCTGGTCAACCG
pHLA-pelB-pgi	pelB_pgi_f1	CCGCTGCTGCTGGTCTGCTGCTCCTCGCTGCCCAGCCGGCGATGGCCATGAAAAACATCAATCCAACGCAGACCG
	XhoI_pgi_re	GCCAAGCTTCTCGAGTTAACCGCGCCACGCTTTATAGCGG
pHLA-pelB-pgi^{H386A}	pgi_H386A_smaI_for	CAGACTGGCCCGATTATCTGGGGTGAACCCGGGACTAACGGTCAGGCCGCGTTCTACCAGCTGATCCACCAGGGAAC
	pgi_H386A_smaI_re	GTTCCCTGGTGGATCAGCTGGTAGAACGCGGCCTGACCGTTAGTCCCGGGTTCACCCCAGATAATCGGGCCAGTCTG
pHLA-pelB-zwf	pelB_zwf_f1	CCGCTGCTGCTGGTCTGCTGCTCCTCGCTGCCCAGCCGGCGATGGCCATGGCGGTAACGCAAACAGCCCAG
	XhoI_zwf_re	GCCAAGCTTCTCGAGTTACTCAAACTCATTCCAGGAACGACCATC

pHLA-pelB-zwf^{H239A}	zwf_H239A_pstI_for	CGGTCAGATGCGCGACATGATCCAGAACGCCCTGCTGCAGATTCTTTGCATGATTGCGATGTCTCCGCC
	zwf_H239A_pstI_re	GGCGGAGACATCGCAATCATGCAAAGAATCTGCAGCAGGGCGTTCTGGATCATGTCGCGCATCTGACCG
pHLA-zwf	no-sig._zwf_Fw	GGAAAAAGGAGATCTGATGGCGGTAACGCAAACAGCCCAG
	no-sig._zwf_Rv	GCCAAGCTTCTCGAGTTACTCAAACTCATTCCAGGAACGACCAT
pHLA-pelB-gfp	gfp_f1	CCGCTGCTGCTGGTCTGCTGCTCCTCGCTGCCCAGCCGGCGATGGCCATGGTGAGCAAGGGCGAGGAGCTG
	gfp_f2	TGGAAAAAGGAGATCTGATGAAATACCTGCTGCCGACCGCTGCTGCTGGTCTGCTGC
	gfp_r	GCCAAGCTTCTCGAGCTACTTGTACAGCTCGTCCATGCCGAGAGTGATC
pHLA-pgi	no-sig._pgi_Fw	GGAAAAAGGAGATCTGATGAAAAACATCAATCCAACGCAGACCG
	no-sig._pgi_Rv	GCCAAGCTTCTCGAGTTAACCGCGCCACGCTTTATAGCG
pSAK-blc-tfu0937	c.n._Tfu0937_f	TCGTCTTCACCTCGAGGCTCCAGATCGCTAGCTTGATCTCTCC
pZA23-blc-tfu0937	c.n._Tfu0937_r	ATTCGATATCAAGCTTCATTTATCAGGGTTATTGTCTCATGAGCGGATAC
pZA23-EIIB^{Glc}	pZ_EIIB_f	TTAAAGAGGAGAAAGGTACC ATGGCGACTGAAGATGCAAAAGCGACAG
	pZ_EIIB_r	ATTCGATATCAAGCTCTATTAGTGGTTACGGATGTACTCATCCATCTCGG
pZA23-EIIC^{Glc}	pZ_EIIC_f	TTAAAGAGGAGAAAGGTACC ATGTTTAAGAATGCATTTGCTAACCTGCAAAAGG
	pZ_EIIC_r	ATTCGATATCAAGCTCTATTAGTCTTCACGACCCGGCGTTTTCAG
pTΔptsG	sgRNA ptsG Fw	GATTGGTTCTGCAATCCAGCTAGCATTATACCTAGGACTGAGCTAGCTGTCAAGG
	sgRNA ptsG Rv	GATTGCAGAACCAATCGGGGTTTTAGAGCTAGAAATAGCAAGTTAAAATAAGGC
	HomSeq Up ptsG Fw	TGCTTTTTTTGAATTCGCTTAGATGCCCTGTACACGGCGAG
	HomSeq Up ptsG Rv	CTGTCTGGTGGCTTCCACCGGAGATAATCCCTCCGAGTACGC
	HomSeq Dw ptsG Fw	GAGGGATTATCTCCGGTGGAAGCCACCAGACAGTTTACCCGCAGTC

	HomSeq Dw ptsG Rv	GCTTCTGCAGGTCGACCTGATCCACTTTAGACAC ATCAGCAACGC
pTΔcrr	sgRNA crr Fw	GCTGGAAGAGAAAGCCAAGCTAGCATTATACCTA GGACTGAGCTAGCTGTCAAGG
	sgRNA crr Rv	GGCTTTCTCTTCCAGCAGGGTTTTAGAGCTAGAA ATAGCAAGTTAAAATAAGGC
	HomSeq Up crr Fw	TGCTTTTTTTGAATTCTTGCTGGCGATGAACGTGC TACACTTC
	HomSeq Up crr Rv	GATAACCGGGGTTTCACCCGGCACGTCTTCGATA TTGACGATCTC
	HomSeq Dw crr Fw	GAAGACGTGCCGGGTGAAACCCCGGTTATCCGCA TCAAGAAGT
	HomSeq Dw crr Rv	GCTTCTGCAGGTCGACGATCTCGACAGTGCCATT GCTGCCG
pTΔpheA	sgRNA pheA Fw	CCATTGTTTGTTGGTCTCGTTTTAGAGCTAGAAAT AGCAAGTTAAAATAAGGCTAGTCCG
	sgRNA pheA Rv	ACCAACAAACAATGGTCACTCGTATTATACCTAG GACTGAGCTAGCTGTCAAGGATCCAG
	HomSeq Up pheA Fw	TGCTTTTTTTGAATTCTACCGTTTTTCTTCGCATTC TTTTTTACCT
	HomSeq Up pheA Rv	TCAGACACGTTACTAGTGCCTGCTGAGTTAATAC GGAATCTTCAA
	HomSeq Dw pheA Fw	ACTCAGCAGGCACTAGTAACGTGTCTGATCAGGT TCCGGC
	HomSeq Dw pheA Rv	AATAGATCTAAGCTTATACGCACAGCGTTTTCAG AGTGAA
pTΔsgrS	sgRNA sgrS Fw	AGTCAACTTTCAGAATTGGTTTTAGAGCTAGAAA TAGCAAGTTAAAATAAGGCTAGTCCG
	sgRNA sgrS Rv	TTCTGAAAGTTGACTTGACTCGTATTATACCTAGG ACTGAGCTAGCTGTCAAGGATCCAG
	HomSeq Up sgrS Fw	TCGGTGCTTTTTTTGAATTCGTCTTCCGCCCGCTG TTGCT
	HomSeq Up sgrS Rv	GCGCGGCGAGACTAGTGACTTAATATAGGGAAA ATAAAATTGCTGTCTTTTGCACAG
	HomSeq Dw sgrS Fw	CCCTATATTAAGTCACTAGTCTCGCCGCGCTAAA AAGGGAACG
	HomSeq Dw sgrS Rv	AGGGTAATAGATCTAAGCTTAGCACACCACAGGT GATAAGCGTC
pTΔpgi	sgRNA pgi Fw	CCCAGAACTCGAACATGTGTTTTAGAGCTAGAAA TAGCAAGTTAAAATAAGGCTAGTCCG
	sgRNA pgi Rv	TGTTCGAGTTCTGGGACACTCGTATTATACCTAG GACTGAGCTAGCTGTCAAGGATCCAG

	HomSeq Up pgi Fw	TCGGTGCTTTTTTTGAATTCTCACTGAAGAGACGC TGGCGA
	HomSeq Up pgi Rv	AAGAAATTGTTACTAGTGCACTTCCGCGATGTGA GTCC
	HomSeq Dw pgi Fw	CGCGGAAGTGCACTAGTAACAATTTCTTTGGTGC GGAAACTGA
	HomSeq Dw pgi Rv	AGGGTAATAGATCTAAGCTTCGGCACCACGTAGT CAAGCG
pTtrpE::tyr^{fbr}	sgRNA trpE Fw	GCTGCCAGTGGTTTCCGTGCTAGCATTATACCTA GGACTGAGCTAGCTGTCAAGG
	sgRNA trpE Rv	GGAAACCACTGGCAGCGGGGTTTTAGAGCTAGA AATAGCAAGTTAAAATAAGGC
	HomSeq Up trpE Fw	TGCTTTTTTTGAATTCGCAATCAGATACCCAGCCC GCCTAATGAG
	HomSeq Up trpE Rv	GGGTGAAATCGCGGCCGCCACAAGGTCATAAGA GAACAGGCCGCCG
	HomSeq Dw trpE Fw	GACCTTGTGGCGGCCGCGATTTCACCCTATTTGG CGCGTCGC
	HomSeq Dw trpE Rv	GCTTCTGCAGGTCGACGTGGCGATACCGTTTTCC ACCAGC
	tyr_ins Fw	GGGTGAAATCGCGGCCGCCCCAGTCTTTCGACTG AGCCTTTCG
	tyr_ins Rv	GACCTTGTGGCGGCCGCATAGGCGTATCACGAGG CCCTTTCGTC
pTptsG::galP-glk	pTptsG_inv.Fw	CCGCCCTAGACCTAGGGACTGCGGGTAAACTGTC TGGTGGCTTC
	pTptsG_inv.Rv	GCTCACAATTCTCGAGCACCGGAGATAATCCCTC CGAGTACGC
	galP-glk_ins Fw	CTCGAGAATTGTGAGCGGATAACAATTGACATTG TGAG
	galP-glk_ins Rv	CCTAGGTCTAGGGCGGCGGATTTGTC
Real-time PCR primers for *mdoG*	mdoG_Fw	TTGCACGACTCTAACGGTCT
	mdoG_Rv	TTCCATGGAGAAGCTGCTGA
Real-time PCR primers for *uhpT*	uhpT_Fw	TCTTTGCGTTGGGTTTCCTG
	uhpT_Rv	TGGCAAAGCTGTCACCAATC

Table S3. Plasmids construction

Products	Primers or Restriction enzymes	Template	Methods
fragment 1	E388A_for E388A_re	pHLA-blc-Tfu0937	PCR
pHLA-blc-Tfu0937^{E389A}	-	fragment 1	In-Fusion HD cloning kit
fragment 2	pelB_Tfu0937_f1 Bgl2_pelB_for	pHLA-blc-Tfu0937	PCR
fragment 3	Bgl2_pelB_for XhoI_Tfu0937_re	fragment 2	PCR
fragment 4	*Bgl*II *Xho*I	pHLA	Restriction enzyme digestion
pHLA-pelB-Tfu0937	- -	fragment 3 fragment 4	In-Fusion HD cloning kit
fragment 5	n.s._tfu0937_f n.s._tfu0937_r	pHLA-blc-Tfu0937	PCR
pHLA-Tfu0937	-	fragment 5 fragment 4	In-Fusion HD cloning kit
fragment 6	Tfu0937-FLAG_Fw Tfu0937-FLAG_Rv	pHLA-blc-Tfu0937	PCR
pHLA-blc-Tfu0937-FLAG	-	fragment 6	In-Fusion HD cloning kit
fragment 7	Tfu0937-FLAG_Fw Tfu0937-FLAG_Rv	pHLA-pelB-Tfu0937	PCR
pHLA-pelB-Tfu0937-FLAG	-	fragment 7	In-Fusion HD cloning kit
fragment 8	Tfu0937-FLAG_Fw Tfu0937-FLAG_Rv	pHLA-Tfu0937	PCR
pHLA-Tfu0937-FLAG	-	fragment 8	In-Fusion HD cloning kit
fragment 9	phoA_f phoA_r	*E. coli* MG1655 genomic DNA	PCR
pHLA-phoA	-	fragment 8 fragment 4	In-Fusion HD cloning kit
fragment 10	phoA_S124A_f	pHLA-phoA	PCR

	phoA_S124A_r		
pHLA-phoA^{S124A}	-	fragment 10	In-Fusion HD cloning kit
fragment 11	pelB_pgi_f1 XhoI_pgi_re	*E. coli* MG1655 genomic DNA	PCR
pHLA-pelB-pgi	-	fragment 11 fragment 4	In-Fusion HD cloning kit
fragment 12	pgi_H386A_smaI_for pgi_H386A_smaI_re	pHLA-pelB-pgi	PCR
pHLA-pelB-pgi^{H386A}	-	fragment 12	In-Fusion HD cloning kit
fragment 13	no-sig._pgi_Fw no-sig._pgi_Rv	pHLA-pelB-pgi	PCR
pHLA-pgi	-	fragment 13	In-Fusion HD cloning kit
fragment 14	pelB_zwf_f1 XhoI_zwf_re	*E. coli* MG1655 genomic DNA	PCR
pHLA-pelB-zwf	-	fragment 14 fragment 4	In-Fusion HD cloning kit
fragment 15	zwf_H239A_pstI_for zwf_H239A_pstI_re	pHLA-pelB-zwf	PCR
pHLA-pelB-zwf^{H239A}	-	fragment 15	In-Fusion HD cloning kit
fragment 16	no-sig._zwf_Fw no-sig._zwf_Rv	pHLA-pelB-zwf	PCR
pHLA-zwf	-	fragment 16	In-Fusion HD cloning kit
fragment 17	zwf-FLAG_Fw zwf-FLAG_Rv	pHLA-pelB-zwf	PCR
pHLA-pelB-zwf-FLAG	-	fragment 17	In-Fusion HD cloning kit
fragment 18	zwf-FLAG_Fw zwf-FLAG_Rv	pHLA-zwf	PCR
pHLA-zwf-FLAG	-	fragment 18	In-Fusion HD cloning kit
fragment 19	zwf_H239A_pstI_for zwf_H239A_pstI_re	pHLA-pelB-zwf-FLAG	PCR

pHLA-pelB-zwf^{H239A}-FLAG	-	fragment 19	In-Fusion HD cloning kit
fragment 20	gfp_f1 gfp_r	pEGFP	PCR
fragment 21	gfp_f2 gfp_r	fragment 20	PCR
pHLA-pelB-gfp	-	fragment 21 fragment 4	In-Fusion HD cloning kit
fragment 22	c.n._tfu0937_f c.n._tfu0937_r	pHLA-blc-Tfu0937	PCR
fragment 23	*Hind*III *Xho*I	pSAK	Restriction enzyme digestion
pSAK-blc-Tfu0937	-	fragment 22 fragment 23	In-Fusion HD cloning kit
fragment 24	Tfu0937-FLAG_Fw Tfu0937-FLAG_Rv	pSAK-blc-Tfu0937	PCR
pSAK-blc-Tfu0937-FLAG	-	fragment 24	In-Fusion HD cloning kit
fragment 25	*Hind*III *Xho*I	pZA23MCS	Restriction enzyme digestion
pZA23-blc-Tfu0937	-	fragment 22 fragment 25	In-Fusion HD cloning kit
fragment 26	Tfu0937-FLAG_Fw Tfu0937-FLAG_Rv	pZA23-blc-Tfu0937	PCR
pZA23-blc-Tfu0937-FLAG	-	fragment 26	In-Fusion HD cloning kit
fragment 27	pZ_EIIB_f pZ_EIIB_r	*E. coli* MG1655 genomic DNA	PCR
fragment 28	*Hind*III *Kpn*I	pZA23MCS	Restriction enzyme digestion
pZA23-EIIB^{Glc}	-	fragment 27 fragment 28	In-Fusion HD cloning kit
fragment 29	pZ_EIIC_f pZ_EIIC_r	*E. coli* MG1655 genomic DNA	PCR
pZA23-EIIC^{Glc}	-	fragment 29	

		fragment 28	In-Fusion HD cloning kit
N20 fragment ptsG	sgRNA ptsG Rv sgRNA ptsG Fw	pTargetF	PCR
pTΔptsGF	-	N20 fragment ptsG	In-Fusion HD cloning kit
H.S. fragment ptsG Up	HomSeq Up ptsG Fw HomSeq Up ptsG Rv	*E. coli* MG1655 genomic DNA	PCR
H.S. fragment ptsG Dw	HomSeq Dw ptsG Fw HomSeq Dw ptsG Rv	*E. coli* MG1656 genomic DNA	PCR
H.S. fragment ptsG	HomSeq Up ptsG Fw HomSeq Dw ptsG Rv	H.S. fragment ptsG Up H.S. fragment ptsG Dw	PCR
pTΔptsGF fragment	*Hind*III *EcoR*I	pTΔptsGF	Restriction enzyme digestion
pTΔptsG	- -	H.S. fragment ptsG pTΔptsGF fragment	In-Fusion HD cloning kit
N20 fragment crr	sgRNA crr Rv sgRNA crr Fw	pTargetF	PCR
pTΔcrrF	-	N20 fragment crr	In-Fusion HD cloning kit
H.S. fragment crr Up	HomSeq Up crr Fw HomSeq Up crr Rv	*E. coli* MG1655 genomic DNA	PCR
H.S. fragment crr Dw	HomSeq Dw crr Fw HomSeq Dw crr Rv	*E. coli* MG1656 genomic DNA	PCR
H.S. fragment crr	HomSeq Up crr Fw HomSeq Dw crr Rv	H.S. fragment crr Up H.S. fragment crr Dw	PCR
pTΔcrrF fragment	*Hind*III *EcoR*I	pTΔcrrF	Restriction enzyme digestion
pTΔcrr	- -	H.S. fragment crr pTΔcrrF fragment	In-Fusion HD cloning kit
N20 fragment pheA	sgRNA pheA Rv sgRNA pheA Fw	pTargetF	PCR

pTΔpheAF	-	N20 fragment pheA	In-Fusion HD cloning kit
H.S. fragment pheA Up	HomSeq Up pheA Fw HomSeq Up pheA Rv	*E. coli* MG1655 genomic DNA	PCR
H.S. fragment pheA Dw	HomSeq Dw pheA Fw HomSeq Dw pheA Rv	*E. coli* MG1656 genomic DNA	PCR
H.S. fragment pheA	HomSeq Up pheA Fw HomSeq Dw pheA Rv	H.S. fragment pheA Up H.S. fragment pheA Dw	PCR
pTΔpheAF fragment	*Hind*III *EcoR*I	pTΔpheAF	Restriction enzyme digestion
pTΔpheA	- -	H.S. fragment pheA pTΔpheAF fragment	In-Fusion HD cloning kit
N20 fragment sgrS	sgRNA sgrS Rv sgRNA sgrS Fw	pTargetF	PCR
pTΔsgrSF	-	N20 fragment sgrS	In-Fusion HD cloning kit
H.S. fragment sgrS Up	HomSeq Up sgrS Fw HomSeq Up sgrS Rv	*E. coli* MG1655 genomic DNA	PCR
H.S. fragment sgrS Dw	HomSeq Dw sgrS Fw HomSeq Dw sgrS Rv	*E. coli* MG1656 genomic DNA	PCR
H.S. fragment sgrS	HomSeq Up sgrS Fw HomSeq Dw sgrS Rv	H.S. fragment sgrS Up H.S. fragment sgrS Dw	PCR
pTΔsgrSF fragment	*Hind*III *EcoR*I	pTΔsgrSF	Restriction enzyme digestion
pTΔsgrS	- -	H.S. fragment sgrS pTΔsgrSF fragment	In-Fusion HD cloning kit
N20 fragment pgi	sgRNA pgi Rv sgRNA pgi Fw	pTargetF	PCR
pTΔpgiF	-	N20 fragment pgi	In-Fusion HD cloning kit
H.S. fragment pgi Up	HomSeq Up pgi Fw		PCR

	HomSeq Up pgi Rv	*E. coli* MG1655 genomic DNA	
H.S. fragment pgi Dw	HomSeq Dw pgi Fw HomSeq Dw pgi Rv	*E. coli* MG1656 genomic DNA	PCR
H.S. fragment pgi	HomSeq Up pgi Fw HomSeq Dw pgi Rv	H.S. fragment pgi Up H.S. fragment pgi Dw	PCR
pTΔpgiF fragment	*Hind*III *EcoR*I	pTΔpgiF	Restriction enzyme digestion
pTΔpgi	- -	H.S. fragment pgi pTΔpgiF fragment	In-Fusion HD cloning kit
N20 fragment trpE	sgRNA trpE Rv sgRNA trpE Fw	pTargetF	PCR
pTΔtrpEF	-	N20 fragment trpE	In-Fusion HD cloning kit
H.S. fragment trpE Up	HomSeq Up trpE Fw HomSeq Up trpE Rv	*E. coli* MG1655 genomic DNA	PCR
H.S. fragment trpE Dw	HomSeq Dw trpE Fw HomSeq Dw trpE Rv	*E. coli* MG1656 genomic DNA	PCR
H.S. fragment trpE	HomSeq Up trpE Fw HomSeq Dw trpE Rv	H.S. fragment trpE Up H.S. fragment trpE Dw	PCR
pTΔtrpEF fragment	*Hind*III *EcoR*I	pTΔtrpEF	Restriction enzyme digestion
pTΔtrpE	- -	H.S. fragment trpE pTΔtrpEF fragment	In-Fusion HD cloning kit
fragment 30	tyr_ins Fw tyr_ins Rv	pSAK-*tyrA*^{fbr}	PCR
fragment 31	*Spe*I	pTΔtrpE	Restriction enzyme digestion
pTtrpE::tyrfbr	-	fragment 30 fragment 31	In-Fusion HD cloning kit
fragment 32	pTptsG_inv.Fw pTptsG_inv.Rv	pTΔptsG	PCR
fragment 32	galP-glk_ins Fw		PCR

	galP-glk_ins Rv	CFT1 genomic DNA	
pTptsG::galP-glk	-	fragment 32 fragment 33	In-Fusion HD cloning kit

SI References

Fujiwara, R., Noda, S., Tanaka, T., Kondo, A., 2020. Metabolic engineering of *Escherichia coli* for shikimate pathway derivative production from glucose–xylose co-substrate. Nat. Commun. 11, 1–12. https://doi.org/10.1038/s41467-019-14024-1

Noda, S., Shirai, T., Mori, Y., Oyama, S., Kondo, A., 2017. Engineering a synthetic pathway for maleate in *Escherichia coli*. Nat. Commun. 8, 1153. https://doi.org/10.1038/s41467-017-01233-9

Noda, S., Shirai, T., Oyama, S., Kondo, A., 2016. Metabolic design of a platform *Escherichia coli* strain producing various chorismate derivatives. Metab. Eng. 33, 119–129. https://doi.org/10.1016/j.ymben.2015.11.007

Tanaka, T., Kawabata, H., Ogino, C., Kondo, A., 2011. Creation of a cellooligosaccharide-assimilating *Escherichia coli* strain by displaying active beta-glucosidase on the cell surface via a novel anchor protein. Appl. Environ. Microbiol. 77, 6265–70. https://doi.org/10.1128/AEM.00459-11